Planform geometry, stacking pattern, and extrabasinal origin of low strength and intermediate strength cohesive debris flow deposits in the Marnoso-arenacea Formation, Italy

P.J. Talling[1,*], G. Malgesini[1,2], E.J. Sumner[1], L.A. Amy[3], F. Felletti[2], G. Blackbourn[4], C. Nutt[5], C. Wilcox[5], I.C. Harding[6,1], and S. Akbari[6,1]

[1]*National Oceanography Centre, European Way, Southampton SO14 3ZH, UK*
[2]*Dipartimento di Scienze della Terra, Università degli Studi di Milano, Via Mangiagalli 34, 20133 Milano, Italy*
[3]*Saudi Aramco, EXPEC Building, Dhahran, 31311, Saudi Arabia*
[4]*Blackbourn Geo-Consulting, Carriden House, Carriden, West Lothian EH51 9SN, UK*
[5]*Department of Earth Sciences, University of Bristol, Queens Road, Bristol BS8 1RJ, UK*
[6]*School of Ocean and Earth Science, University of Southampton, European Way, Southampton SO14 3ZH, UK*

ABSTRACT

The Miocene Marnoso-arenacea Formation (Italy) is the only ancient sequence where deposits of individual submarine density flow deposits have been mapped in detail for long (>100 km) distances, thereby providing unique information on how such flows evolve. These beds were deposited by large and infrequent flows in a low-relief basin plain. An almost complete lack of bed amalgamation aids bed correlation, and resembles some modern abyssal plains, but contrasts with ubiquitous bed amalgamation seen in fan-lobe deposits worldwide. Despite the subdued topography of this basin plain, the beds have a complicated character. Previous work showed that a single flow can commonly comprise both turbidity current and cohesive mud-rich debris flows. The debris flows were highly mobile on low gradients, but their deposits are absent in outcrops nearest to source. Similar hybrid beds have been documented in numerous distal fan deposits worldwide, and they represent an important process for delivering sediment into the deep ocean. It is therefore important to understand their origin and flow dynamics. To account for the absence of debrites in proximal Marnoso-arenacea Formation outcrops, it was proposed that debris flows originated within the study area due to erosion of mud-rich seafloor; we show that this is incorrect. Clast and matrix composition show that sediment within the cohesive debris flows originated outside the study area.

Previous work showed that intermediate and low strength debris flows produced different downflow-trending facies tracts. Here, we show that intermediate strength debris flows entered the study area as debris flows, while low strength (clast poor) debris flows most likely formed through local transformation from an initially turbulent mud-rich suspension. New field data document debrite planform shape across the basin plain. Predicting this shape is important for subsurface oil and gas reservoirs. Low strength and intermediate strength debrites have substantially different planform shapes. However, the shape of each type of debrite is consistent. Low strength debrites occur in two tongues at the margins of the outcrop area, while intermediate strength debrite forms a single tongue near the basin center. Intermediate strength debrites are underlain by a thin layer of structureless clean sandstone that may have settled out from the debris flow at a late stage, as seen in laboratory experiments, or been deposited by a forerunning turbidity current that is closely linked to the debris flow. Low strength debrites can infill relief created by underlying dune crests, suggesting gentle emplacement. Dewatering of basal clean sand did not cause a long runout of debris flows in this location. Hybrid beds are common in a much thicker stratigraphic interval than was studied previously, and the same two types of debrite occur there. Hybrid flows transported large volumes (as much as 10 km^3 per flow) of sediment into this basin plain, over a prolonged period of time.

*Email: Peter.Talling@noc.ac.uk.

INTRODUCTION

Submarine sediment density flows dominate sediment transport into many parts of the deep ocean, and produce some of the most extensive and voluminous sediment accumulations on Earth. Their deposits form thick sequences in the rock record that can contain major oil and gas reserves (Nielsen et al., 2007). It is the scale of these underwater sediment flows that is often remarkable, with very large volumes of sediment spread across tens to hundreds of kilometers of low gradient seafloor. Individual flow deposits (beds) in the Miocene Marnoso-arenacea Formation of Italy contain 1–10 km^3 of sediment (Talling et al., 2007a, 2007b). This sediment volume is similar to the annual sediment flux from all of the world's modern rivers (Milliman and Syvitski, 1992). These submarine flows were at least 30 km wide, and most likely 60 km wide (Ricci-Lucchi and Valmori, 1980; Amy and Talling, 2006; Talling et al., 2007a, 2007b). For comparison, the Amazon River is ~10 km wide where it meets the sea. Each bed considered in this study has been mapped out across an area of 120 × 30 km in the northern Apennine mountain belt between 109 separate rock outcrops (Fig. 1; Amy and Talling, 2006; Talling et al., 2007a, 2007b). This is the only location where individual ancient flow deposits have been mapped out in such detail over such distances; such mapping is important because it documents planform deposit shape and stacking patterns, and how flows evolve spatially.

The Marnoso-arenacea Formation differs from most submarine fan sequences (Nielsen et al., 2007) in that it records infrequent but

Geosphere; December 2012; v. 8; no. 6; p. 1207–1230; doi:10.1130/GES00734.1; 17 figures; 2 tables; 1 supplemental figure file.
Received 27 June 2011 ♦ Revision received 22 February 2012 ♦ Accepted 14 May 2012 ♦ Published online 18 October 2012

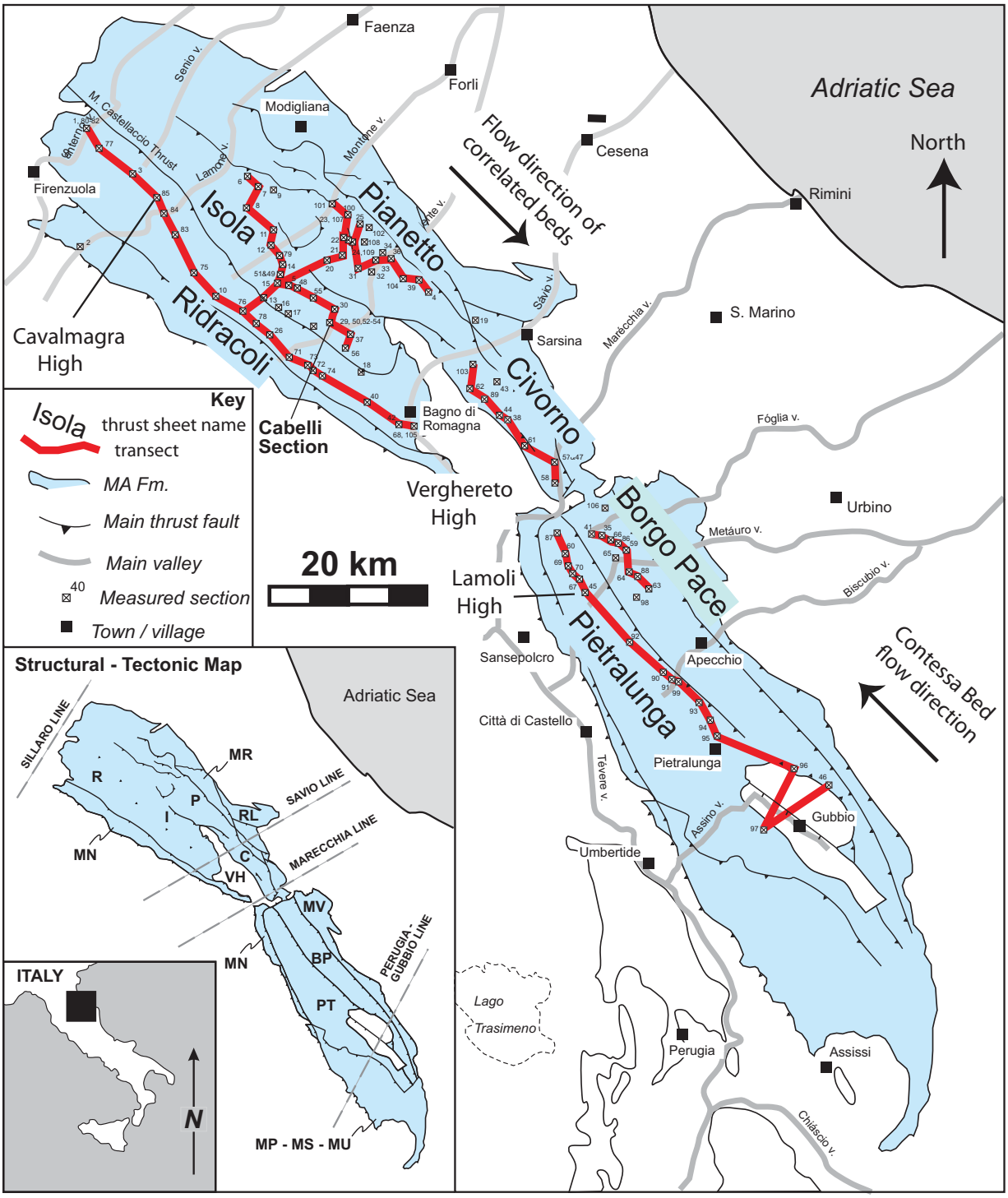

Figure 1. Location map for the Marnoso-arenacea Formation (MA Fm.) outcrop that shows the position of measured sections. The name and exact global positioning system location of each numbered section was documented in Amy and Talling (2006; web Table 1 therein). Postdepositional thrust faults subdivide the outcrop area into a number of thrust sheets, which are shown on the inset map. These are the Ridracoli (R), Monte Nero (MN), Isola (I), Pianetto (P), Civorno (C), Rullato (RL), Pietralunga (PT), Borgo Pace (BP), Monte Vicino (MV), Monte Roncole (MR), and Monte de Portole–Monte Salaiole–Monte Urbino (MP-MS-MU) elements. The position of the intrabasinal Verghereto high (VH) and a series of transverse tectonic lines are also shown on the inset map. The Lamoli and Cavalmagra highs are small topographic features (Talling et al., 2007a). Red lines indicate downflow transects of correlated sections along the Ridracoli, Isola, Pianetto, Civorno, Borgo Pace, and Pietralunga thrust sheets (see Figs. 2–4, 9–14; Supplemental Figs. 1–3 in the Supplemental Figure File [see footnote 1]). An across-flow transect of sections spanning the Ridracoli, Isola and Pianetto thrust sheets (see Fig. 9D) is also indicated by a red line. Figure modified from Talling et al. (2007b).

particularly large volume flow events, thus facilitating bed correlation. It lacks the ubiquitous bed amalgamation seen in lobe sequences worldwide (Nielsen et al., 2007; Hodgson, 2009) that are most likely fed by much more frequent flows. The Marnoso-arenacea Formation resembles deposits cored in modern deep-water (abyssal) basin plains fed by large and infrequent flows (Reeder et al., 2000; Wynn et al., 2002; Talling et al., 2007c; Frenz et al., 2008). Such abyssal plain sequences tend to be on oceanic crust (unlike the Marnoso-arenacea Formation), and subduction of oceanic crust may reduce their likelihood of preservation in the rock record.

We originally chose the Marnoso-arenacea Formation for study because it was deposited in a low-gradient basin plain and has a relatively simple morphology; it lacks channels or evidence for commonplace flow reflection, and there is almost no bed amalgamation (Figs. 2–4; Ricci-Lucchi and Valmori, 1980; Amy and Talling, 2006; Talling et al., 2007a, 2007b, 2012a, 2012b; Sumner et al., 2012). We therefore thought that deposit geometries would be relatively simple and easily compared to conceptual or numerical models. However, even in such a simple depositional setting, it is now apparent that the submarine flows were actually remarkably complicated, and differ in key regards from widely cited models (e.g., Lowe, 1982) that predict flow evolution and deposit geometry in downflow transects (Talling et al., 2007a, 2012a, 2012b; Sumner et al., 2012).

Perhaps the most notable difference is that most of the larger volume beds comprised both turbidity current and mud-rich (cohesive) debris flow deposits (Amy and Talling, 2006). Such hybrid or linked turbidite-debrite beds were described previously (e.g., Wood and Smith, 1958; Hiscott and Middleton, 1979, 1980; Ricci-Lucchi and Valmori, 1980; Zeng et al., 1991), but only recently has it become apparent that they are common in many locations worldwide (Haughton et al., 2003, 2009; Sylvester and Lowe, 2004; Talling et al., 2004, 2007c, 2010; Amy and Talling, 2006; Ito, 2008; Zeng et al., 1991; Amy et al., 2009; Hodgson, 2009; Jackson et al., 2009; Pyles and Jennette, 2009; Muzzi Magalhaes and Tinterri, 2010). Understanding these hybrid flows is important because they are a common feature of the most important processes for delivering sediment to the deep ocean. It is also important to predict their occurrence, location, and internal geometry in subsurface oil and gas reservoirs in order to extract those petroleum reserves most effectively, because mud-rich debrite sandstones have much lower permeability and poorer reservoir quality than the clean turbidite sandstones (Amy et al., 2009).

Terminology

Herein we consider sandstone intervals that have a relatively high interstitial mud matrix, and are therefore inferred to be deposited by debris flows with significant cohesive strength (Talling et al., 2004, 2012a; Amy and Talling, 2006; Haughton et al., 2009). The longer term "mud-rich sandy debris flow" is shortened here to "mud-rich debris flow," and "mud-rich debrite sandstone" is shortened to "mud-rich debrite." The terms mud-rich and cohesive are used synonymously. It is important to distinguish these mud-rich debrites from clean sandstones with lower interstitial mud contents that have been attributed to debris flow deposition (Shanmugam and Moiola, 1995; Talling et al., 2012b).

Previous Work

Ricci-Lucchi and Valmori (1980) showed that it was possible to correlate thicker beds in the Marnoso-arenacea Formation for long distances within an ~200-m-thick stratigraphic interval that contains the Contessa megaturbidite marker bed. They logged 18 sections at a scale of 1:50, noting the presence of clast-rich "slurried beds" that they attributed to erosion within the outcrop area and local bed amalgamation. Amy and Talling (2006) presented a much more detailed bed correlation framework for a narrower 30-m-thick interval of strata above the Contessa bed; 109 sections were logged at a scale of 1:10. The thinner beds were relogged in more detail (1:5; Talling et al., 2007a) and it was shown that many thin beds could also be correlated across the entire 120 × 30 km outcrop area; the logged sections cover all 7 major thrust sheets (which were termed structural elements in past work) (Fig. 1).

In Amy et al. (2005) and Amy and Talling (2006), it was shown that the ~30 m interval above the Contessa bed contained two types of mainly ungraded mud-rich sandstone deposited en masse by cohesive debris flow. The first type of cohesive debrite contains abundant clasts and tends to pinch out abruptly (facies tract 2), while cohesive debrites that lack clasts or have very small clasts taper gradually into graded silty mud in more distal settings (facies tract 3). The rate of clast-rich debrite thinning is between 13 and 39 cm/km; clast-poor debrites and clean turbidite sandstones thin at rates of <5 cm/km. It was concluded (Amy and Talling, 2006) that both types of cohesive debris flow probably originated through erosion of underlying muddy seafloor within the outcrop area, such that the increased mud concentration within the flow damped turbulence; it was proposed that debris flows therefore most likely resulted from flow transformation from turbidity currents within the basin plain.

Collection of New Field Data

This contribution is based on a substantial amount of new field work representing over 1 person-year in the field. The thick beds in the stratigraphic interval above the Contessa bed have been relogged in more detail at a scale of 1:5 in 86 of the 109 sections. More detailed information has been collected on paleocurrent directions (including within the bed), and mud-clast composition and maximum length. The (>800) new paleocurrent measurements augment >2200 paleocurrent measurements (summarized in Amy and Talling, 2006; Talling et al., 2007a). An unusually large number (311) of thin section analyses were used to quantify variations in sand grain size and matrix mud content (cf. Sylvester and Lowe, 2004); data from 108 of these thin sections were published previously (Amy and Talling, 2006; Talling et al., 2007a). Sandstone composition was investigated in 54 thin sections. The abundance of organic carbon was measured for different lithologies in selected beds in the interval above the Contessa bed.

Beds were then correlated within a second ~80-m-thick stratigraphic interval below the Contessa bed, between 28 sections logged at a scale of 1:10 or 1:5 (Talling et al., 2012b). The total number of beds analyzed increased from 56 to 93. A continuous ~600 m section in which every bed is exposed was logged at Cabelli at a scale of 1:10. The frequency and types of mud-rich cohesive debrites in this longer section and the two correlated intervals were compared in order to see if the correlated intervals were representative of the wider interval.

AIMS

The first aim of this contribution is to describe the types of mud-rich debrites and hybrid beds within the newly studied and thicker stratigraphic interval. Is the thicker stratigraphic interval characterized by just two types of clast-rich and clast-poor mud-rich debrite, as documented by Amy and Talling (2006)? Are mud-rich debrites just as frequent in the thicker stratigraphic interval, as in the thinner interval studied by Amy and Talling (2006)? The second aim is to describe the planform geometry and the stacking pattern of mud-rich debrites within the above-Contessa interval. What is the planform shape and stacking pattern of the different types of mud-rich debrites? Do the planform shape and stacking pattern show system trends that could help to predict the location, extent, and relative abundance of mud-rich debrites in other sequences? The third aim is to determine the origin of the different types of

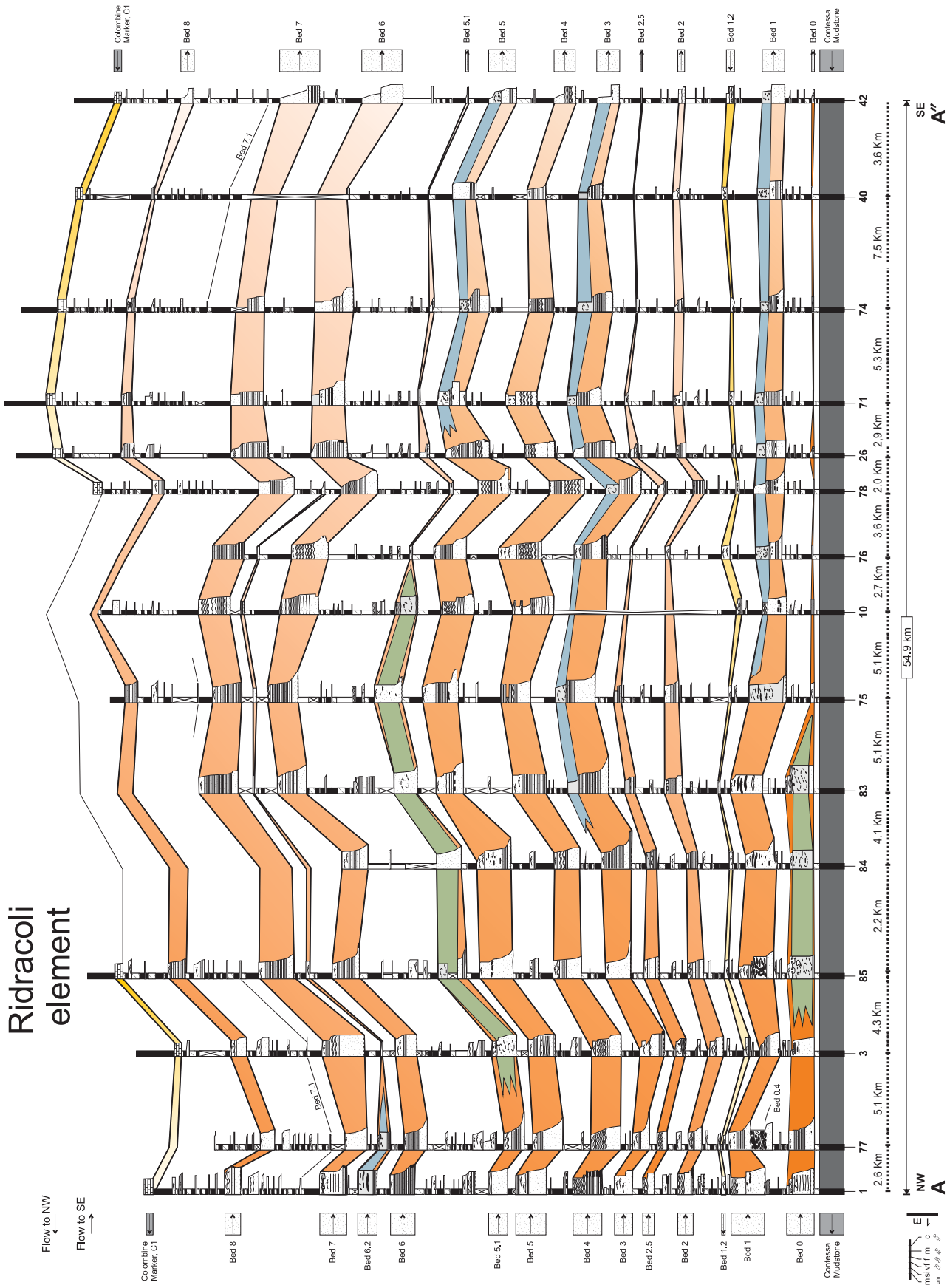

Figure 2. Correlation of thick beds within a stratigraphic interval above the Contessa megaturbidite, along the Ridracoli thrust sheet. The locations of transect and numbered sections are shown in Figure 1. Colors denote muddy debrite sandstone (blue—facies MS1 and MS2), clean turbidite sandstone (orange—facies CS1–CS6), and clean debrite sandstone (dark green—CS7) within thicker beds. Paleoflow was subparallel to the trend of transect. Most of the beds were deposited by flow from the northwest (from left to right), although a small number of beds (shown in yellow) traversed the basin plain from the opposite direction. Figure modified from Amy and Talling (2006).

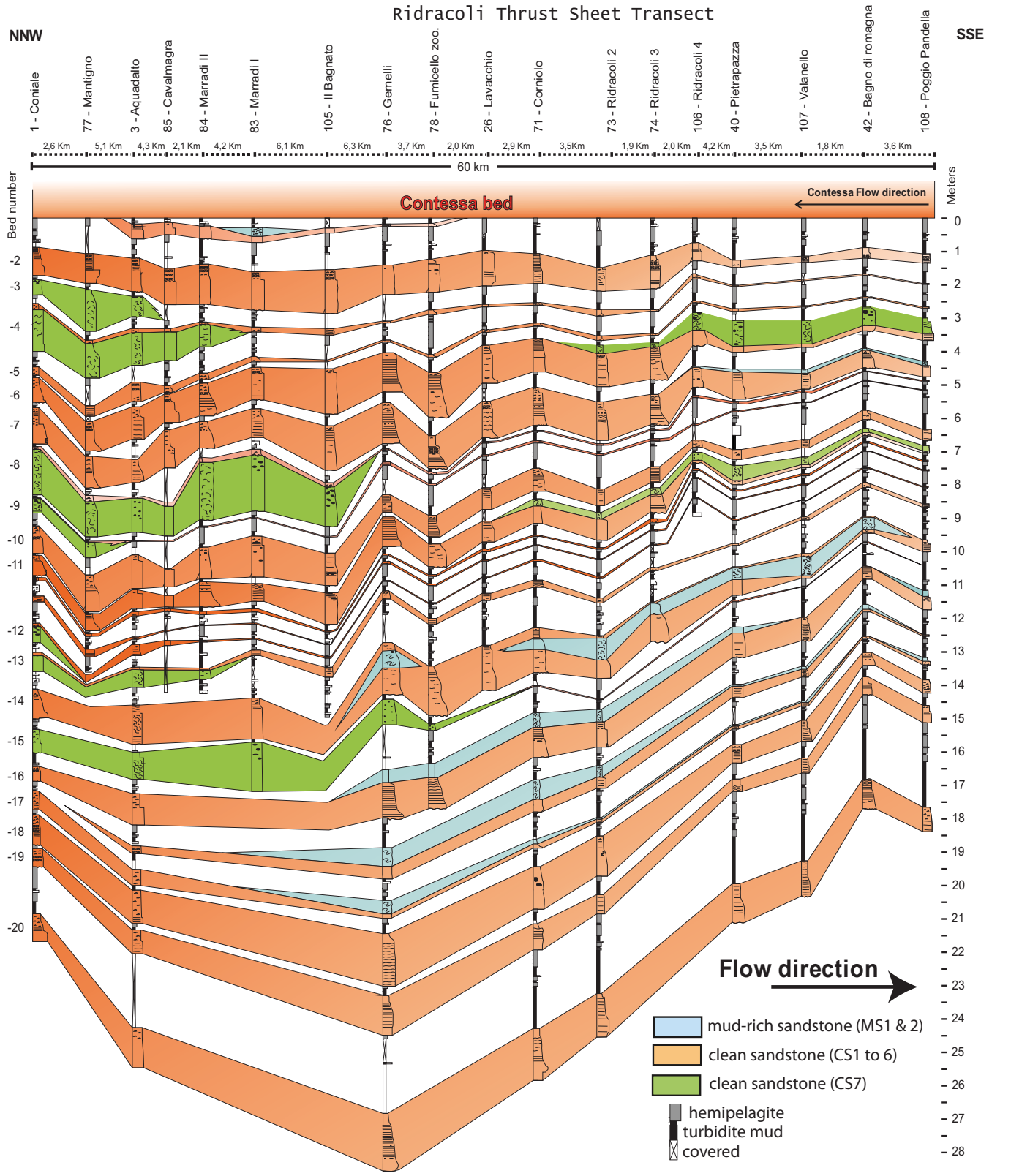

Figure 3. Correlation of thick beds along the Ridracoli thrust sheet within a stratigraphic interval below the Contessa megaturbidite. The locations of transect and numbered sections are shown in Figure 1. Colors denote muddy debrite sandstone (blue—facies MS1 and MS2), clean turbidite sandstone (orange—facies CS1–6), and clean debrite sandstone (dark green— CS7) within thicker beds. Paleoflow was subparallel to the trend of transect. Most of the beds were deposited by flow from the northwest (from left to right), although the Contessa megaturbidite was deposited by flow in the opposite direction.

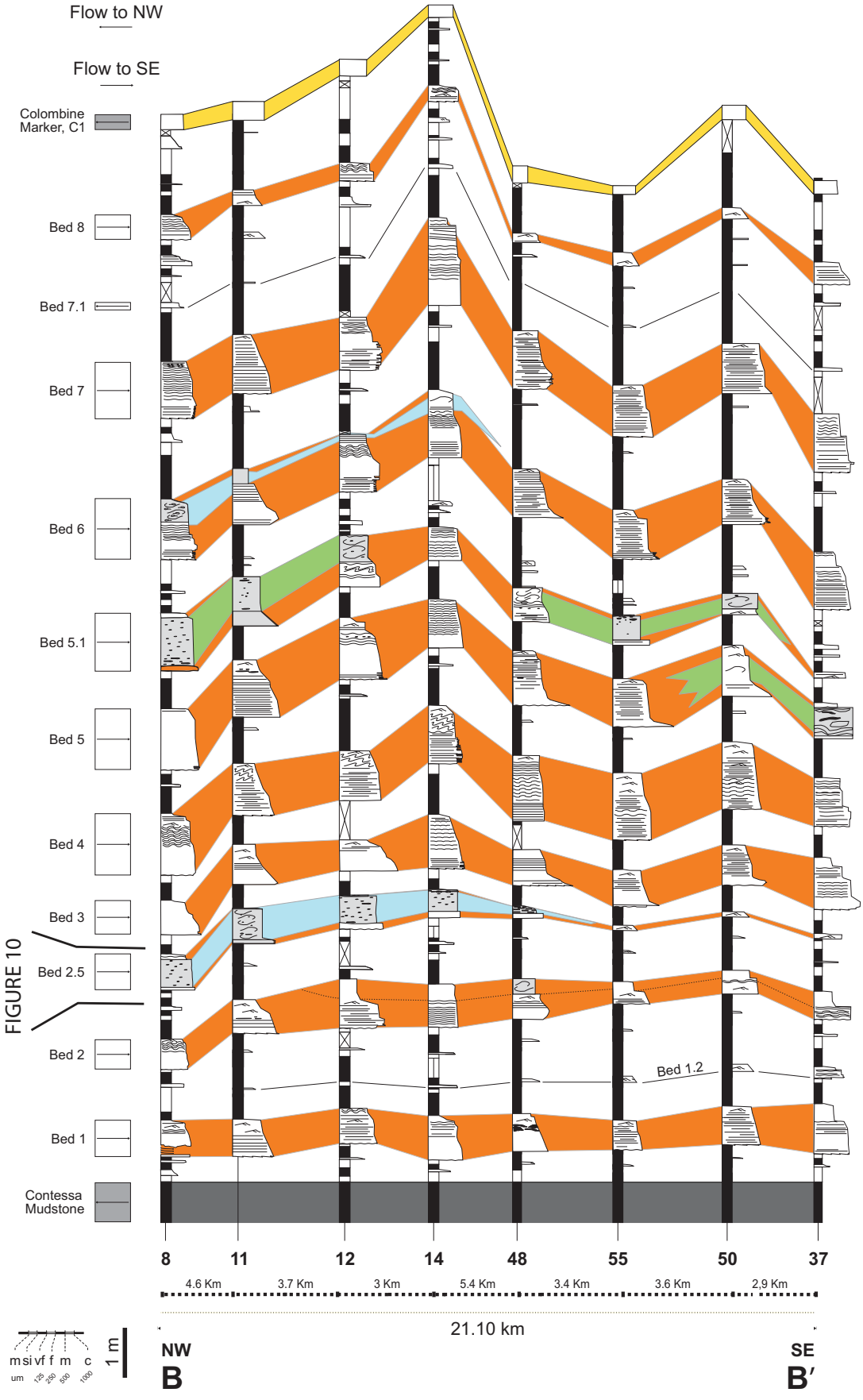

Figure 4. Correlation of thick beds along the Isola thrust sheet within a stratigraphic interval below the Contessa megaturbidite. The locations of transect and numbered sections are shown in Figure 1. Colors denote muddy debrite sandstone (blue—facies MS1 and MS2), clean turbidite sandstone (orange—facies CS1–CS6), and clean debrite sandstone (dark green—CS7) within thicker beds. Paleoflow was subparallel to the trend of transect. Most of the beds were deposited by flow from the northwest (from left to right). The Contessa bed, Colombine-1 bed (shown in yellow), and a small number of other beds (e.g., beds 1.2, 7.1) traversed the basin plain from the opposite direction. Figure modified from Amy and Talling (2006) and Talling et al. (2007a).

mud-rich cohesive debris flows. Did both types of debris flows originate within the basin plain due to erosion of mud-rich seafloor sediment, as suggested by Amy and Talling (2006)? Are the debris flows far travelled from outside the study area, or did they form locally within the basin plain? The final aim is to document the character and infer the depositional process of clean sand intervals found beneath each type of mud-rich debrite. Was this basal clean sand deposited by turbidity currents, or by other processes? Is there evidence that dewatering of the basal clean sand lubricated the cohesive debris flows, and played a major role in their long run out?

METHODS

Bed Correlation Framework and Facies Scheme

Previous publications have described in detail the bed correlation framework for thick (Amy et al., 2005; Amy and Talling, 2006; Talling et al., 2007b) and thin (Talling et al., 2007a) beds in the interval above the Contessa bed. Outcrop logging was originally undertaken at 109 sections at a scale of 1:10 (Amy and Talling, 2006); 86 of these sections were revisited as part of this contribution. More detailed sedimentary logging was undertaken for individual beds at a scale of 1:5; these more detailed sedimentary logs forms the basis for describing bed geometries in downflow transects along all five thrust sheets (Figs. 2–4; Supplemental Figs. 1–6 in the Supplemental Figure File[1]). The methodology used in Amy and Talling (2006) was adopted for logging (at a scale of 1:10) and correlating beds in the stratigraphic interval below the Contessa bed (Fig. 3) and for logging beds (at a scale of 1:10) in the longer section at Cabelli. The facies scheme adopted in this contribution is modified from that presented in Amy and Talling (2006). This scheme classifies sediments hierarchically based on: (1) lithofacies and (2) subfacies (Table 1). Subfacies were distinguished on the basis of sedimentary structures and grading patterns. Lithofacies types include clean sandstones with relatively low matrix-mud content (CS lithofacies) and muddy sandstones with significantly higher matrix-mud fractions (MS lithofacies). Siltstone and mudstone lithofacies are also distinguished (Si and M lithofacies) (Table 1).

Grain-Size Analysis

Grain size was estimated in the field using a grain-size comparator. The term sandstone is adopted for intervals dominated by grains estimated to be coarser than ~125 μm. The size and percentage abundance of finer grains could not be defined reliably in the field using visual observation (Figs. 5 and 6). Mud content, vertical grading patterns, and grain-size distributions were then quantified using thin sections from beds 0, 1, 2.5, 3, and 6 in the interval above the Contessa bed (Fig. 7). Thin sections were used to document vertical grading patterns within beds, typically for a number of adjacent sections in areas that display key changes in lithofacies. Analyses were initially conducted using images from a scanning electron microscope (SEM). The longest axes of the 300 largest grains were counted for each thin section, at different levels within the bed. Grains (mainly micas) having a longest axis more than three times longer than the shortest axis were excluded from these measurements. Mud content was quantified as the percentage area covered by distinct grains having a longest axis shorter than ~32 μm in the SEM images.

Images from an optical microscope were analyzed for a larger set of samples in beds 2.5 and 3 (Figs. 5 and 6). These optical images were found to allow more rapid, if somewhat less detailed, data collection. Mean grain size was determined by measuring the long axis of 300 framework grains, selecting grains at grid points within a thin section. The percentage of grains at these grid points with long axes of <32 μm, as a proportion of clearly detrital grains, defines the mud content of the sample. Thin section analyses measure oblique slices through grains, rather than their true long axis length. Such data suffice to document relative changes in grain size (grading) and mud content.

Paleocurrent Analysis and Basin-Floor Morphology

More than 3000 paleocurrent directions were recorded from the 109 logged sections in the interval above the Contessa bed (Amy and Talling, 2006; Talling et al., 2007a). The vast majority of measurements (>90%) were made from flutes and grooves found on the base of beds. A much smaller number (<80) of paleocurrent measurements were made using corrugated lineations and dune-scale cross-bedding within turbidite sandstone intervals, which were located directly below debrites. These directions are subparallel to the flow directions recorded by basal flutes and grooves. More than 1000 paleocurrent measurements were taken in the Cabelli section and in the strata interval below the Contessa bed, mainly (but not exclusively) from basal flutes and grooves.

The lack of channels and bed amalgamation, together with the extensive sheet-like geometry of both thick and thin beds, indicates deposition in a relatively flat basin plain (Ricci-Lucchi and Valmori, 1980). Relative thinning of the correlated interval of strata indicates the presence of the Verghereto high between the Ridracoli and Pietralunga thrust sheets in the central basin plain (Fig. 1; Ricci-Lucchi and Valmori, 1980; Talling et al., 2007a). The lack of evidence for flow reflection or major changes in paleocurrent direction (Talling et al., 2007a) and the observation that all beds (even beds thinner than 10 cm) are found on both sides of the Verghereto high (Amy and Talling, 2006; Talling et al., 2007a) suggest that the Verghereto high had limited bathymetric relief during the period studied. Two even more subtle paleohighs are suggested by small but consistent changes in sandstone interval thicknesses near the Cavalmagra section on the Ridracoli thrust sheet, and the Lamoli section on the Pietralunga thrust sheet (Talling et al., 2007a). The observation that all of the beds (even the thin beds of <10 cm of turbidite mud) are continuous across both the Cavalmagra and Lamoli highs suggests that these highs had even more limited relief.

The paleocurrent data and spatial changes in bed thickness (even for thin beds) within the correlated interval (Talling et al., 2007a) provide no evidence for ridges oriented along the foredeep axis, parallel to thrust fronts that later shortened the outcrop, as suggested by Muzzi Magalhaes and Tinterri (2010). It is possible (but unlikely) that such bathymetric ridges produced no flow deflection or changes in bed thickness because they were oriented parallel to paleoflow. A decrease in the number of thin beds between the Ridracoli and Isola thrust sheets could be due to such a ridge, but it could

[1]Supplemental Figure File. PDF file of six supplemental figures. In each figure, A is the Pianetto, Civorno, and Borgo Pace thrust sheets; B is the Isola thrust sheet; C is the Ridracoli and Pietralunga thrust sheets; and D is a vertically exaggerated basin-floor relief showing local highs (from Talling et al., 2007b). Supplemental Figure 1: Summary of the architecture of bed 3 in downflow transects along A, B, C, and D. Supplemental Figure 2: Summary of the architecture of bed 2.5 in downflow transects along A, B, C, and D. Supplemental Figure 3: Summary of the architecture of bed 6 in downflow transects A, B, C, and D. Supplemental Figure 4: Summary of the architecture of bed 7 in downflow transects along A, B, C, and D. Supplemental Figure 5: Summary of the architecture of bed 1 in downflow transects along A, B, C, and D. Supplemental Figure 6: Summary of the architecture of bed 2 in downflow transects along A, B, C, and D. If you are viewing the PDF of this paper or reading it offline, please visit http://dx.doi.org/10.1130/GES00734.S1 or the full-text article on www.gsapubs.org to view the Supplemental Figure File.

also simply be due to confinement of smaller volume flows toward the axis of the foredeep. The only evidence of flow reflection in the correlated beds is in turbidite mud (which consistently ponded in the southeastern part of the outcrop area), and within the uppermost sandy part of the Contessa bed, in the three northwesternmost sections in the Santerno Valley (Fig. 1; Ricci Lucchi and Valmori, 1980; our field observations). Such flow reflection in the Contessa bed is unsurprising given that this flow traversed the basin plain in the opposite direction of most other flows (Ricci Lucchi and Valmori, 1980), and therefore most likely flowed uphill for a substantial distance. A more complete analysis of the inferred basin morphology was presented in Talling et al. (2007a).

Compositional Analyses

Optical petrography was used to analyze the composition of mud-rich and clean sandstone, and to determine whether these two types of sandstone came from the same source. Previous studies of the Marnoso-arenacea Formation sandstones used detrital rock fragments to fingerprint different Alpine and Apennine sources for clean turbidite sandstone (Gandolfi et al., 1983). However, these distinctive rock fragments only occur in coarse sandstone. Mud-rich sandstone is finer grained than the samples used by Gandolfi et al. (1983), and lacks such coarse grain sizes. The composition of detrital sediment within finer grained sandstone was found to be strongly dependent on grain size, primarily reflecting how grain shape and settling velocity depend on composition. Micas and foraminiferal fragments, in particular, are much more common in finer sandstone intervals. For this reason, a qualitative analysis of sandstone composition was first made using a wide range of samples. Clean sandstone and mud-rich sandstone samples with a similar mean grain size were then compared qualitatively in one bed.

Total organic carbon (TOC) analyses were produced by homogenizing 15 g of each sample by powdering in an agate mill. Then 1 g of each sample was decarbonated in 10% Analar HCl, followed by further decarbonation in 37% Analar HCl. These samples were decant washed and oven dried at 40 °C. The percent TOC was determined using a Carlo-Erba CE-1108 elemental analyzer calibrated with Imidizole. Analytical precision is ~0.2%.

Attempts were made to analyze benthic foraminifera assemblages to constrain the water depths at which sediment originated, and hence the origin of turbidity current and debris flow (cf. Talling et al., 2007c). Unfortunately, the

TABLE 1. FACIES SCHEME (REVISED FROM AMY AND TALLING, 2006)

Lithofacies and Subfacies	Grain size: Mud	Slt	Vf. Sand	F. Sand	M. Sand	C. Sand	Thickness: Cm.	Cm. - m	> m.	Description	Interpretation
Cs7: swirly, predominantly ungraded										Swirly weathering and poorly sorted. Generally ungraded. Possibly weakly normally graded in the uppermost part. Sharp grain size break at upper surface. Can contain chaotically distributed mud clasts, and large deformed clasts of sandstone. Patchy texture, with adjacent areas of coarser and finer grains. Thin section analysis confirm similar mud content to other clean sandstone lithofacies.	Rapid deposition or en-masse freezing of a current with relatively high sediment concentration throughout. Flow dominated by grain interactions and/or hindered settling. See Talling et al. (2012b).
MS Lithofacies: Muddy Sandstone Ms1: Matrix supported with floating clasts										Unclean grey hue and sticky when moist. Swirly fabric. Poorly sorted. Ungraded. Matrix supported. Usually <20% clasts. Millimeter to meter sized clasts of mudstone and marl, less commonly sandstone. Size and composition of clasts vary spatially. Often an abundance of micas and organic particles. Upper contact displays a sharp grain size discontinuity.	Cohesive flow with sufficiently high sediment concentrations to inhibit segregation of particles of different sizes; en-masse sedimentation.
Ms2: Matrix supported without floating clasts										Unclean grey hue and sticky texture. Poorly sorted, usually ungraded. Often with an abundance of micas and organic particles. Swirly, sheared-like fabric. Sharp, planar upper contact showing a break in grain size.	Cohesive flow with sufficiently high sediment concentrations to inhibit segregation of particles of different sizes; en-masse sedimentation.
Si Lithofacies: Siltstone Si1: Laminated										Planar or undular parallel laminated "fissile" silt. Often contains large amounts of organic fragments and mm-sized platelets of mica.	Deposition from a traction-dominated flow-boundary zone beneath a dilute and turbulent current. Equivalent to Bouma Td (Bouma, 1962).
Si2: unstructured normally graded										Graded interval often found between very-fine sand and mud at the top of sandstone beds. Often contains large amounts of organic fragments and micas. Displays a gradual grading at its upper surface.	Suspension fall-out under waning flow conditions. A dilute flow that was fully turbulent throughout.
Si3: unstructured and ungraded (massive)										Featurless silt often found at the top of sandstone beds. Often contains large amounts of organic fragments and mm-sized platelets of micas. Similar to Ms2 but finer.	A) Suspension fall-out under waning flow conditions. A dilute flow that was fully turbulent throughout. B) A current with a basal flow boundary dominated by grain interactions and/or cohesion and/or hindered settling.
M Lithofacies: Mudstone M1: massive dark (turbidite/debrite) mud										Grey color, darker than marl. Devoid of structures or grading.	Suspension fall-out from a static or slow-moving mud cloud probably involving a fluid mud layer. Final deposition from a sediment gravity flow event. Equivalent to Bouma Te division (Bouma, 1962).

(*continued*)

TABLE 1. FACIES SCHEME (REVISED FROM AMY AND TALLING, 2006) (*continued*)

Lithofacies and Subfacies	Grain size: Mud	Slit	Vf. Sand	F. Sand	M. Sand	C. Sand	Thickness: Cm.	Cm. - m	> m.	Description	Interpretation
M2: massive calcareous (hemipelagite) mud										Light grey bluish, calcareous, speckled appearance containing white foraminifer tests. Massive.	Settling of individual hemipelagic particles from the overlying water column.
CS: Clean SandstoneLithofacies Cs1: Ripple cross-laminated										Thin laminae (< 3 mm), commonly convolute or wavy Interval normally grade or ungraded. Common in thin (< 40 cm) sandstones and in the upper part of m-thick sandstones.	Deposition from a traction-dominated flow-boundary zone. The current was sufficiently dilute to form ripples; relatively dilute and turbulent throughout. Equivalent to Bouma Tc division (Bouma, 1962).
Cs2: Dune cross laminated										Occur in thick sandstone beds typically near the top of the bed, common below MS intervals. 1-2 mm thick laminae. Bed forms have wave-lengths between 0.2-0.9 m normally graded or ungraded clean sandstone interval. Isolated or climbing dune bedforms.	Deposition from a traction-dominated flow-boundary zone. The current was sufficiently dilute to form bedforms. Relatively dilute and turbulent throughout. (Dune scale cross-lamination of Ricci-Lucchi and Valmori (1980); see their fig. 4).
Cs3: parallel lamination - planar or gently undulating										Occur in thick sandstone beds typically above Cs5 and Cs6, and below Cs1 or Cs2. Typically 1 mm or less thick (unlike Cs6). Normally graded clean sandstone intervals.	Deposition from a thin near bed zone with high sediment concentration dominated by grain to grain interactions. Lamination formed by repeated collapse of high concentration near bed layers or by traction within upper stage planar bed regime. Equivalent to Bouma Tb division (Bouma, 1962).
Cs4: parallel to sub-parallel "stepped grain size" statification										Cm thick stratification or >5 mm thick laminae displaying step-like normal or inverse grading patterns. Occasional low angle wavy surfaces or truncations. usually at the base of thick and coarse sandstone beds.	A) Deposition from an unsteady traction-dominated flow boundary beneath a relatively dilute and turbulent current. B) Deposition from a modified grainflow layer under unsteady flow conditions. Successive traction bed load grain layers (traction carpet sedimentation). SGF with a basal flow boundary dominated by grain interactions and/or hindered settling. Equivalent to Lowe S2 division (Lowe, 1982).
Cs5: Unstructured normally graded										Grading pattern may be subtle (< 1 phi). Common in thick and thin sandstone beds. Usually located at the base of the bed, or separated from base of bed by a ripple cross laminated interval. Gradual grading at upper interval boundary.	Rapid suspension fall-out from a waning current with near bed zone dominated by grain to grain interactions. Overlying flow can be dilute and fully turbulent. Structureless deposits can form by repeated collapse of high concentration near bed layers. Equivalent to Bouma Ta (Bouma, 1962).
Cs6: Unstructured and ungraded (massive)										Devoid of structure or grading. Sharp grain size break at upper surface. Thin section analysis confirm similar mud content as other clean sandstone intervals.	A) "Suspension fall-out" from a steady current that is relatively dilute and turbulent throughout. B) Rapid deposition or "en-masse freezing" of a current with relatively high concentration where the basal flow boundary is dominated by grain interactions and/or hindered settling.

samples were too well indurated for successful disaggregation of foraminifera (M. Rogerson and T. Kouwenhoven, 2008, personal commun.).

RESULTS

Different Types of Mud-Rich (Cohesive) Debrite and Hybrid Bed

The wider stratigraphic interval contains the same two types of mud-rich debrite intervals and hybrid-bed facies tracts that were seen in the interval above the Contessa bed (Amy and Talling, 2006; Figs. 5 and 6). Both types of cohesive debrite have a predominantly ungraded mud-rich sand matrix, with detrital fine mud (<32 μm) contents in excess of ~15% (Figs. 5–7). This ungraded mud-rich matrix records en masse consolidation by cohesive mud-rich debris flow, such that larger and smaller grains do not segregate. (See Talling et al. [2004], Amy et al. [2005], Amy and Talling [2006], and Talling et al. [2007a, 2007c] for a fuller description of how deposition from cohesive debris flow is inferred.) The upper few centimeters of the debrite can show normal grading (Fig. 5B), and this is attributed to mixing and dilution with overlying seawater. The upper boundary of the muddy debrite sandstone is always a sharp grain-size break, which can be overlain by either turbidite mud or rippled sandstone (Figs. 5 and 6).

Clast-Poor Mud-Rich Debrite Sandstone (Deposited by Low Strength Cohesive Debris Flow)

The more common type of mud-rich debrite interval is typically 20–60 cm thick, and contains either no mud clasts or very small (<5 mm) mud clasts (Figs. 5, 8, 9A, 9D, 11, and 12). This type of clast-poor debrite is characteristically underlain by a relatively thick interval of graded turbidite clean sandstone, which typically displays planar, wavy-parallel (crenulated) or dune-scale cross-lamination (Fig. 5). In some cases, the mud-rich debrite sandstone infills relief associated with underlying dune crests (Fig. 5C). The mud-rich debrite sandstone grades laterally downflow into even finer grained graded muddy silt (Supplemental Figs. 1–3 in the Supplemental Figure File [see footnote 1]). Two intervals of mud-rich debrite, separated by a few centimeters of rippled sand, are seen in parts of bed 7.

The absence or small size of mud clasts suggests relatively low strength, as does the passive infilling of dune crests (Fig. 5C). Lateral grading into muddy silt may result from progressive dilution of the low strength debris flow as it mixes relatively easily with surrounding seawater (Talling et al., 2002).

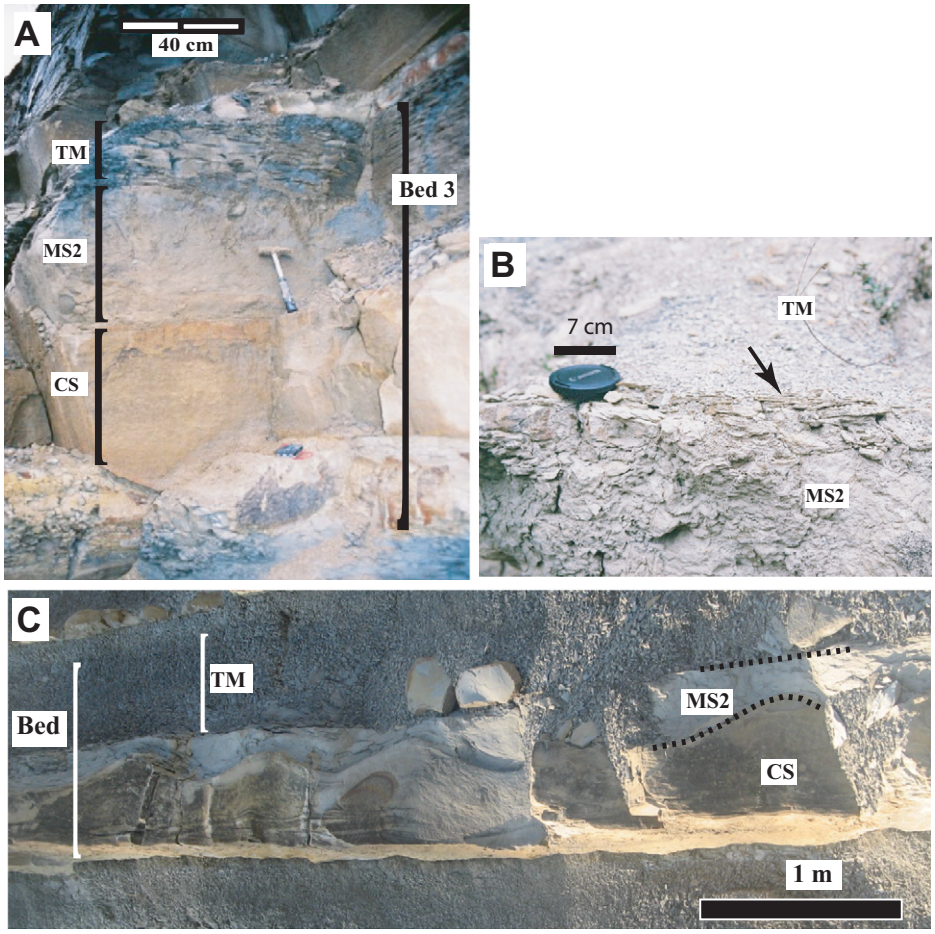

Figure 5. Outcrop photographs of beds containing mud-rich sandstone intervals lacking clasts (MS2). (A) Bed 3 at the Galeata section 2 comprising turbidite mudstone (TM), ungraded mud-rich sandstone (MS2), and normally graded clean sandstone that is structureless, planar-laminated, or dune-scale cross-laminated (CS—clean sandstone). The base of the bed has deep linear grooves. Grain size and matrix-mud content were measured using scanning electron microscope images of thin sections. (B) Sharp surface (arrowed) that separated mud-rich sandstone without clasts (MS2) from overlying turbidite mudstone (TM) in bed 7 at the Fiumicello Zootechnica section. (C) Bed from section below the Contessa bed at the Castel del Priore section comprising turbidite mudstone (TM), mud-rich sandstone lacking clasts (MS2), and basal clean sandstone (CS). The mud-rich sandstone infills dune crests at the top of the basal clean sandstone, indicating slow emplacement of the mud-rich sandstone by low strength cohesive debris flow.

Clast-Rich Mud-Rich Debrite Sandstone (Deposited by Intermediate Strength Cohesive Debris Flow)

The second type of mud-rich debrite is 30–120 cm thick, and contains abundant mud clasts (Fig. 6). The mud clasts can range from a few centimeters to several meters in length, and are rounded or subrounded (Fig. 6). The mud-rich debrite interval is characteristically underlain by a thinner interval of structureless sandstone, which may be separated from a much finer interval of ripple cross-laminated sand by a grain-size break. The clast-rich mud-rich debrite interval and underlying structureless clean sand terminate abruptly in the same location in bed 2.5 (Fig. 10). The basal ripple cross-laminated interval appears at the base of the bed just before this abrupt termination (Fig. 10). The mud-rich debrite intervals, which are not seen on the Ridracoli transect in the interval of correlated beds (Figs. 2 and 3), extend upflow to the most proximal outcrops on the Isola thrust sheet (Fig. 4). There is no location where a clast-rich debrite could be mapped upflow into a bed comprising only turbidite sand and mud.

The larger clast size and abrupt termination indicate that this type of mud-rich debris flow most likely had a higher strength, although the debris flows were still sufficiently mobile to produce thin deposits across the low-gradient basin plain. The cohesive strength of these debris flows is intermediate between the clast-poor debris flows and clast-rich debris flow that produce much thicker (tens of meters) mud-rich debrites in other locations (Piper et al., 1999; Laberg and Vorren, 2000). The interval of ripple cross-laminated sand that appears near the pinch-out of the cohesive debrite may result from abrupt deceleration of a debris flow (Fig. 10). It is inferred that a previously trailing dilute turbidity current extended ahead of the rapidly decelerating debris flow, and thereby deposited the ripple cross-laminated interval at the base of the bed.

Lateral Changes Within a Single Bed

Bed correlations show that a single bed can contain both clast-rich (higher strength) and clast-poor (low strength) cohesive debrite in adjacent downflow transects. This cross-flow change is illustrated by beds 2.5 and 3 (Fig. 9; Supplemental Figs. 1 and 2 in the Supplemental Figure File [see footnote 1]), and most likely results from lateral change in debris flow strength. Such variation in strength may result from changes in mud content and degree of mixing with surrounding seawater.

Planform Geometry and Stacking Pattern of Mud-Rich (Cohesive) Debrites

Mud-rich debrites within hybrid beds cover between 15% and 60% of the outcrop area (Fig. 13). They commonly extend for 40 km along the basin in a direction parallel to flow, and can extend for as much as 80 km in such a direction. They commonly extend for at least 10–15 km across the basin (Fig. 13). Mud-rich debrite sandstone intervals were probably even more extensive when deposited, as they are often truncated by the limits of available outcrop, and thrust faulting has reduced the original width of the basin (Fig. 1).

The planform geometry of mud-rich debrite intervals is relatively complicated, but shows a number of trends (Figs. 13 and 14). Mud-rich debrites are most common in the mid-basin, and always absent in the most proximal sections on the Ridracoli thrust sheet, and in the most distal sections on the Pietralunga thrust sheet (Fig. 13). Clast-rich debrites do not occur on the Ridracoli element, and they cannot be tracked upflow into beds only comprising turbidite. They pinch out abruptly either in mid-basin (bed 2.5) or in the more distal basin (bed 5). Clast-poor debrite

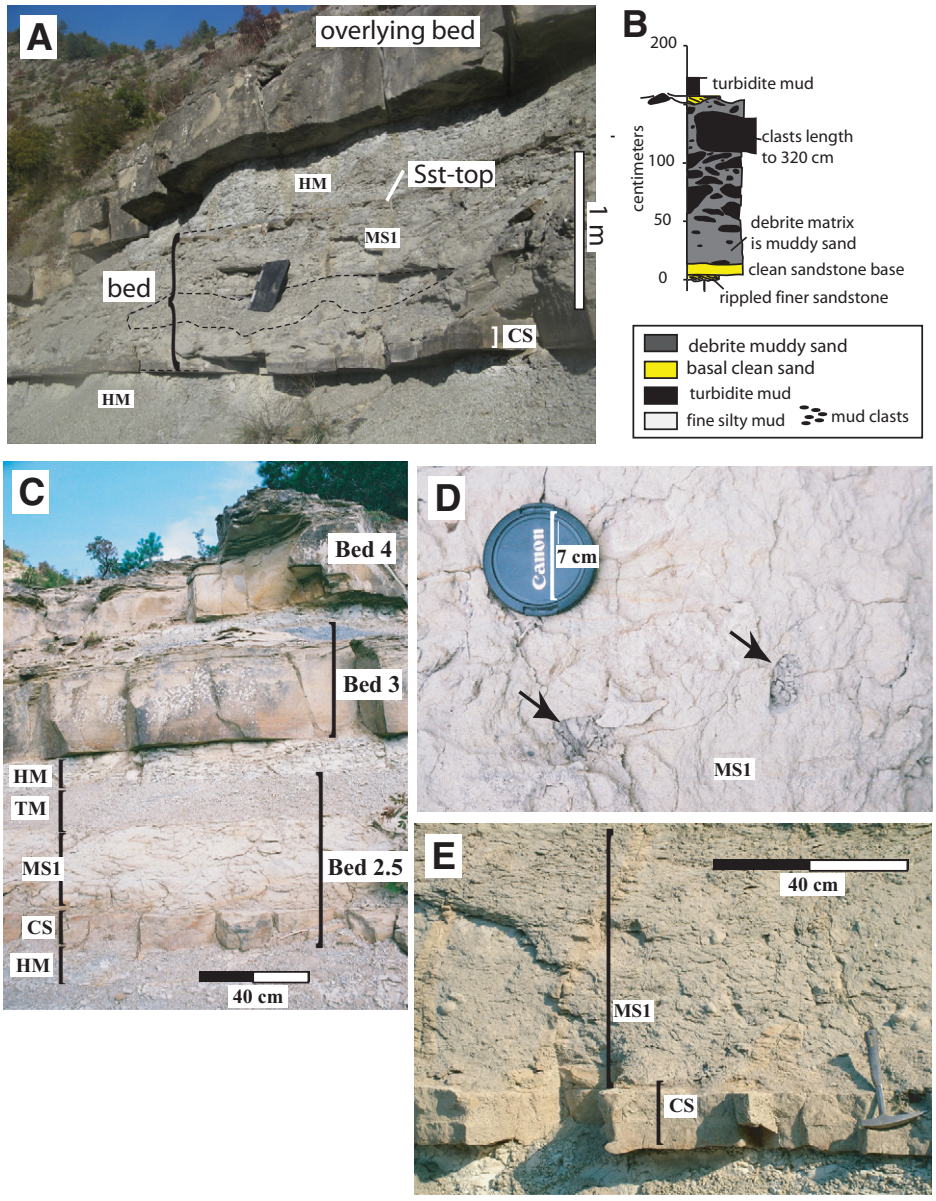

Figure 6. Outcrop photographs of beds containing mud-rich sand intervals with clasts. (A) Thin debris flow deposit with mud-rich sandstone matrix that contains boulder-sized mudstone clasts up to 320 cm in length. The base of the bed comprises a thin layer of clean sand (sandstone, Sst, base). The debrite is overlain by a thin interval of rippled clean sand (Sst, top) and turbidite mud. Bed is several hundred meters below the Contessa bed in the Cabelli-1 section (29) (Amy and Talling, 2006). HM—hemipelagic mudstone; MS1—debrite with mud clasts; TM—turbidite mud; CS—clean sand. (B) Graphic log of the bed shown in panel D. (C) Outcrop photograph showing bed 2.5, which comprises basal clean sand (CS), mud-rich debrite sand with chaotically distributed small mud clasts (MS-1), and overlying turbidite mud (TM). Beds 3 and 4 comprise only turbidite sand and mud at this locality (Monte Roncole section 14; Amy and Talling, 2006). However, bed 3 also comprises mud-rich debrite sandstone elsewhere in the outcrop area, as shown in Figs. 9 and 13. (D) Detailed photographs of clasts in bed 2.5 at Monte Roncole. (E) Bed 3 at the Cigno section (section 4 in Amy and Talling, 2006) showing a muddy debrite sandstone interval with mud clasts (MS-1) underlain by a thin basal interval of clean sand (Fig. 9D).

intervals can be tracked up flow into the sections comprising only turbidite on the Ridracoli transect (Figs. 9, 11, 12, and 13). The low strength cohesive debris flows either bypassed (i.e., without depositing sediment) or were not present in these most proximal sections (discussed herein). The clast-poor (low strength) debrites are best developed in two lobes on the Ridracoli and Pianetto elements (Fig. 13), and are typically absent on the intervening Isola element. This consistent stacking pattern might be related to subtle increases in elevation, but this cannot be tested because bathymetric data are lacking.

Frequency and Clustering of Mud-Rich (Cohesive) Debrites

The 419-m-thick interval logged at Cabelli contains 37 beds with mud-rich debrite sandstone intervals, or 1 debrite sandstone interval per 11.3 m of strata (Fig. 15). The interval of correlated beds above the Contessa bed contains two mud-rich debrite sandstone intervals at Cabelli, or 1 cohesive debrite per 11.1 m of strata. The cumulative thickness of background hemipelagic mudstone was also calculated for both intervals. If hemipelagic accumulation rates did not vary significantly, this cumulative thickness gives a crude estimate of the relative amount of time represented by each interval of strata. The wider stratigraphic interval contains 107.37 m of hemipelagite mudstone, and has 1 mud-rich debrite per 290.2 cm of hemipelagite. The interval of correlated beds has 3.52 m of hemipelagic mudstone, and has 1 debrite sandstone per 176 cm of hemipelagite. Numerous mud-rich debrite sandstones occur within the wider stratigraphic interval, and their frequency is broadly similar to that observed in the Contessa to Colombine-1 stratal interval. The overall impression is that the mud-rich debrite intervals are poorly clustered in the longer Cabelli section (Fig. 15).

Previous work showed that most (7 of 10) larger volume (>0.7 km^3) beds in the correlated interval above the Contessa bed contain mud-rich debrite sandstone at some point within the outcrop area (Talling et al., 2007b). One might therefore expect the majority of larger volume beds in the wider 419-m-thick stratigraphic interval to also contain mud-rich debrites, although further field work would be needed to demonstrate this conclusively.

Character of Mud-Rich (Cohesive) Debrites in the Cabelli Section

The character of beds with mud-rich debrite intervals in the 419-m-thick Cabelli section (Fig. 16) was analyzed to show whether the same two

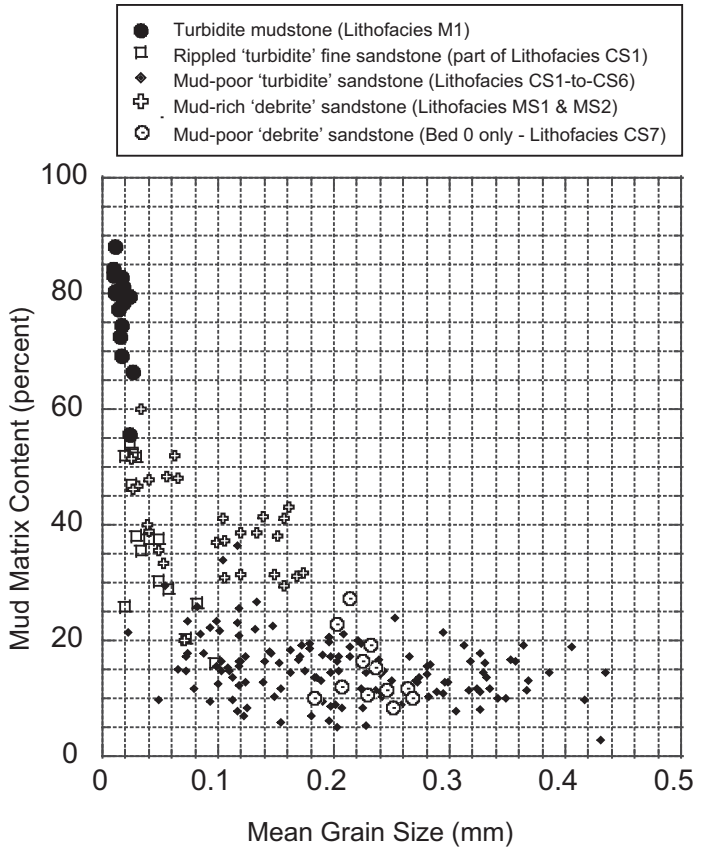

Figure 7. Textural data from different lithofacies from thin section analyses. Mean grain size is based on point-counting the long axis of 300 grains. Mud matrix content is fraction of sample comprising detrital grains finer than 32 μm.

types of debrite occur: (1) clast-poor debrite with thick basal clean sand deposited incrementally by turbidity current (as shown by laminations), and (2) clast-rich debrites with a thin structureless basal sand interval. Clast-poor debrites tend to have thick basal clean sandstones, but this is not always the case (Fig. 16A). The clean sand beneath clast-poor debrites most commonly contains some laminations, providing evidence of deposition by turbidity current (Fig. 16A), but there are a few exceptions with structureless basal intervals (that could still be deposited by turbidity current). Clast-rich debrites in contrast tend to have thinner clean-sand bases, most commonly without any laminations (Fig. 16A), as is case for bed 2.5. The relative thickness of basal clean sand to the thickness of the overlying mud-rich debrite shows a clear trend, when compared to maximum clast size in the mud-rich debrite (Fig. 16B). Mud-rich debrites with larger clasts have a basal clean-sand interval that is thinner than the mud-rich debrite. Mud-rich debrite intervals with no clasts are sometimes underlain by much thicker basal clean-sand intervals, although they can also be underlain by thin basal clean-sand intervals. The data from the longer (419 m) Cabelli section (Fig. 16B) are therefore consistent with the hypothesis that beds containing clast-rich and clast-poor mud-rich debrite intervals tend toward the two different geometries seen in the narrower (~30 m) interval of beds that were correlated across the basin plain. Debrites with larger mud clasts also tend to have coarser matrix sand size in the longer Cabelli section, although the grain-size measurements are not very precise because they were made with a grain-size comparator card. This relationship would be consistent with a stronger debrite matrix that is able to support both larger sand grains and larger mud clasts (Fig. 16C).

Muzzi Magalhaes and Tinterri (2010) studied an even wider interval of Marnoso-arenacea Formation strata and concluded that muddy debrite beds (their type 1) are common and resemble the bed geometry and facies tracts described in Amy and Talling (2006). They also described somewhat thicker beds (to 4 m) that contain muddy debrite intervals with even larger clasts (their type 2 beds), which we also observed (Fig. 6A). We do not observe evidence of repeated flow reflection and liquefaction that they attribute to intrabasinal highs (their type 3), but beds comprising turbidite sand and mud (their types 4 and 5) are common.

Composition and Provenance of Sand Grains in Turbidite and Debrites

Both clean sandstones and mud-rich sandstones comprise quartz, alkali feldspar, plagioclase, flakes and aggregates of biotite, muscovite, and chlorite, glauconite, detrital carbonate fragments, small and commonly broken foraminifera, and numerous altered, probably chloritic fragments. Owing to the variety of detrital components observed, several of which have distinctive features, it is unlikely that clean and mud-rich sandstones were derived from substantially different sources. A particularly detailed examination was made for samples with similar mean grain size from clean and mud-rich debrite sandstone in bed 2.5 at Monte Roncole (section 14;

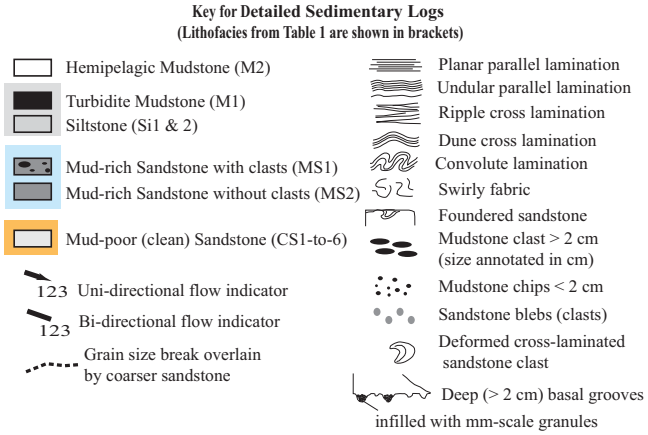

Figure 8. Key to symbols used in Figures 9–13.

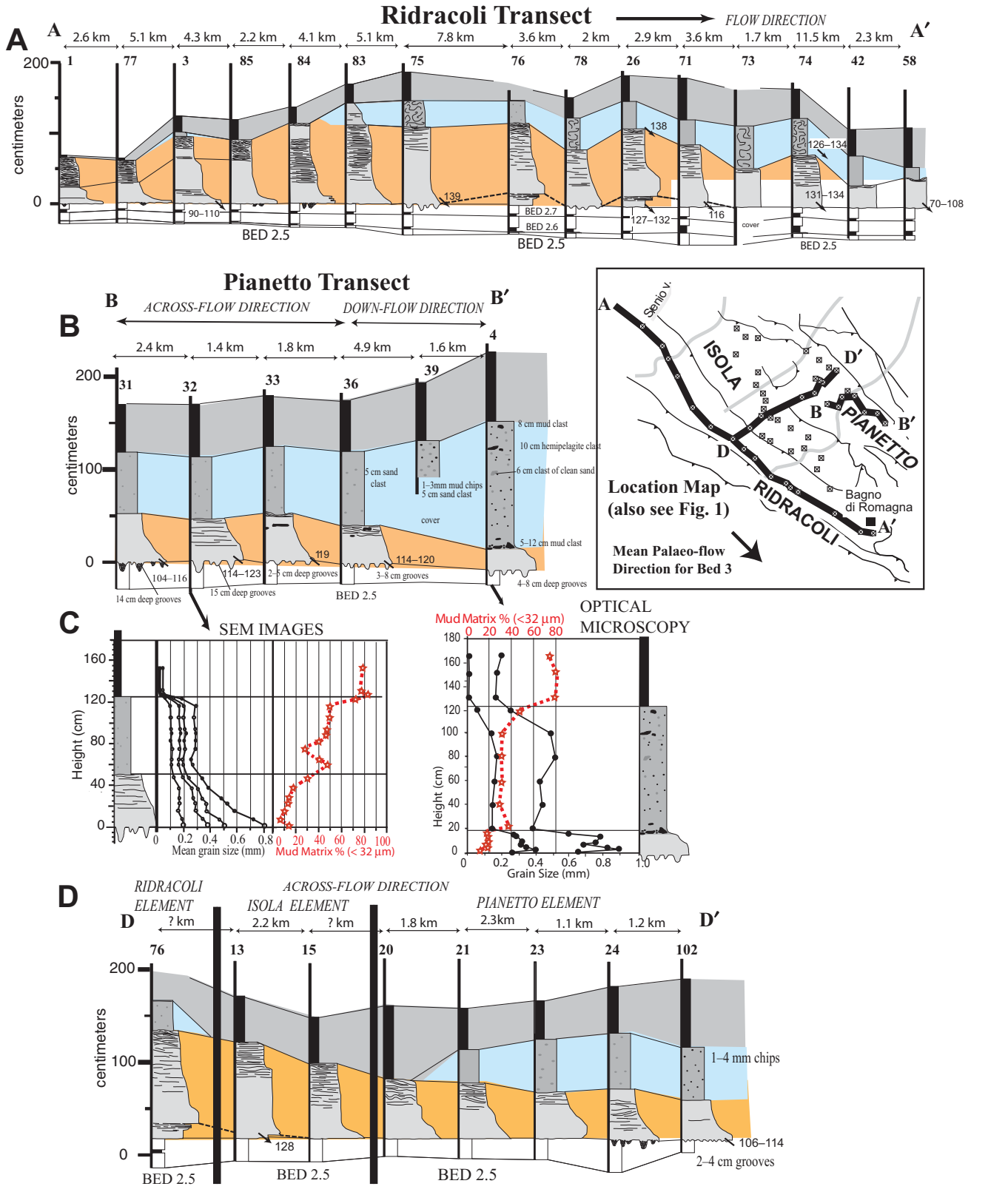

Figure 9. Geometry of bed 3 showing that clast-rich debrite sandstone (MS1) can be laterally equivalent to clast-poor debrite sandstone (MS2), and that debrite sandstone occurs in two tongues within this bed. (A) Downflow transect on Ridracoli thrust sheet (from Talling et al., 2007b). (B) Downflow transect on Pianetto thrust sheet. (C) Grain size and mud content quantified using analyses of optical microscope images (SEM—scanning electron microscope). (D) Transect oriented across flow that spans the Ridracoli, Isola, and Pianetto thrust sheets. Location map for transects is shown by inset panel (also see Fig. 1). For symbol key, see Figure 8.

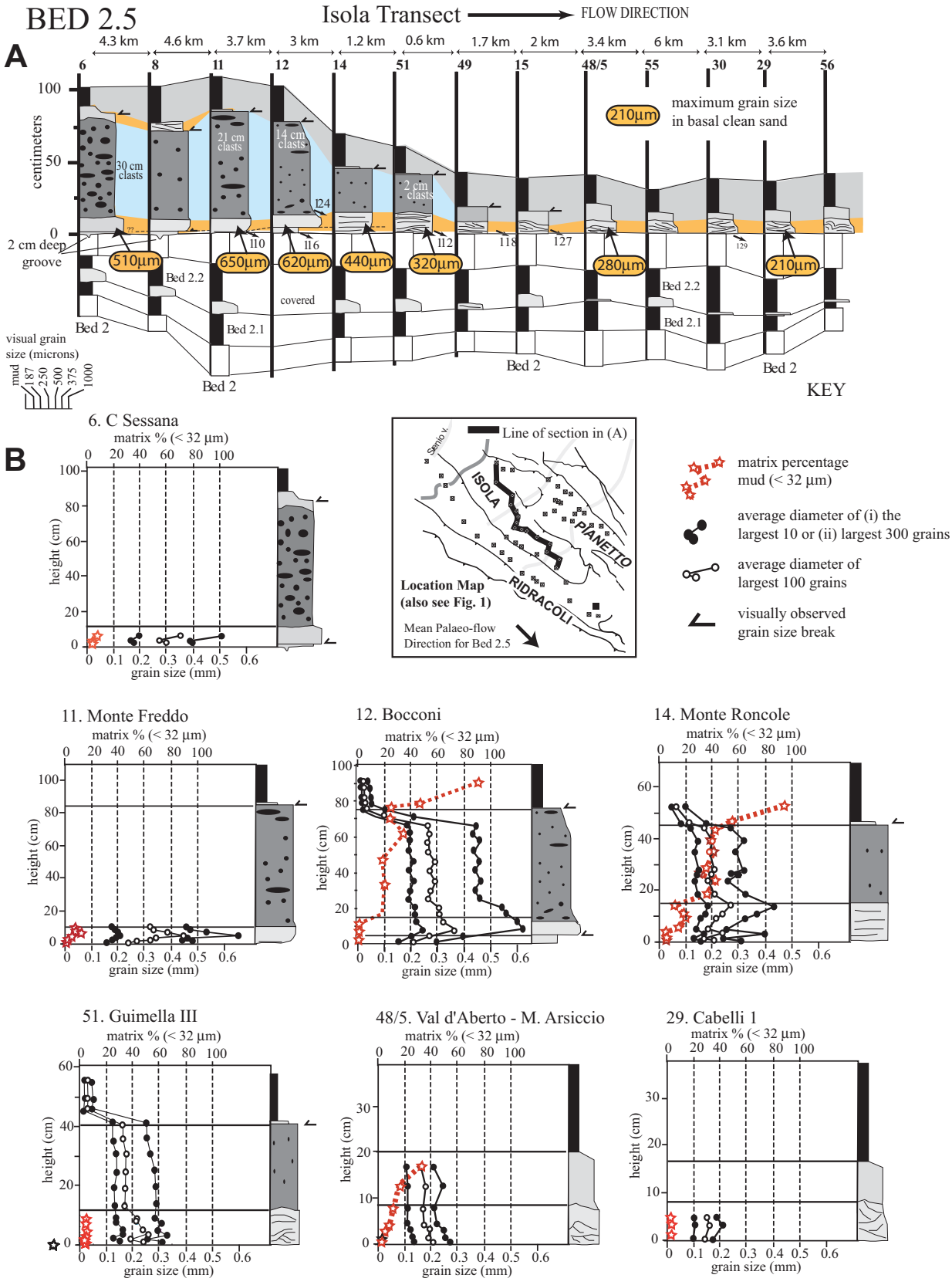

Figure 10. Changes in bed 2.5 in a downflow-oriented transect along Isola thrust sheet (Fig. 1). (A) Bed character, paleocurrent direction, and depth of erosion into underlying strata. (For symbol key, see Figure 8.) (B) Grain size and mud content quantified using scanning electron microscope images or optical microscope images. (For photos of bed 2.5 at Monte Roncole [section 14] [Amy and Talling, 2006], see Figs. 6C, 6D.)

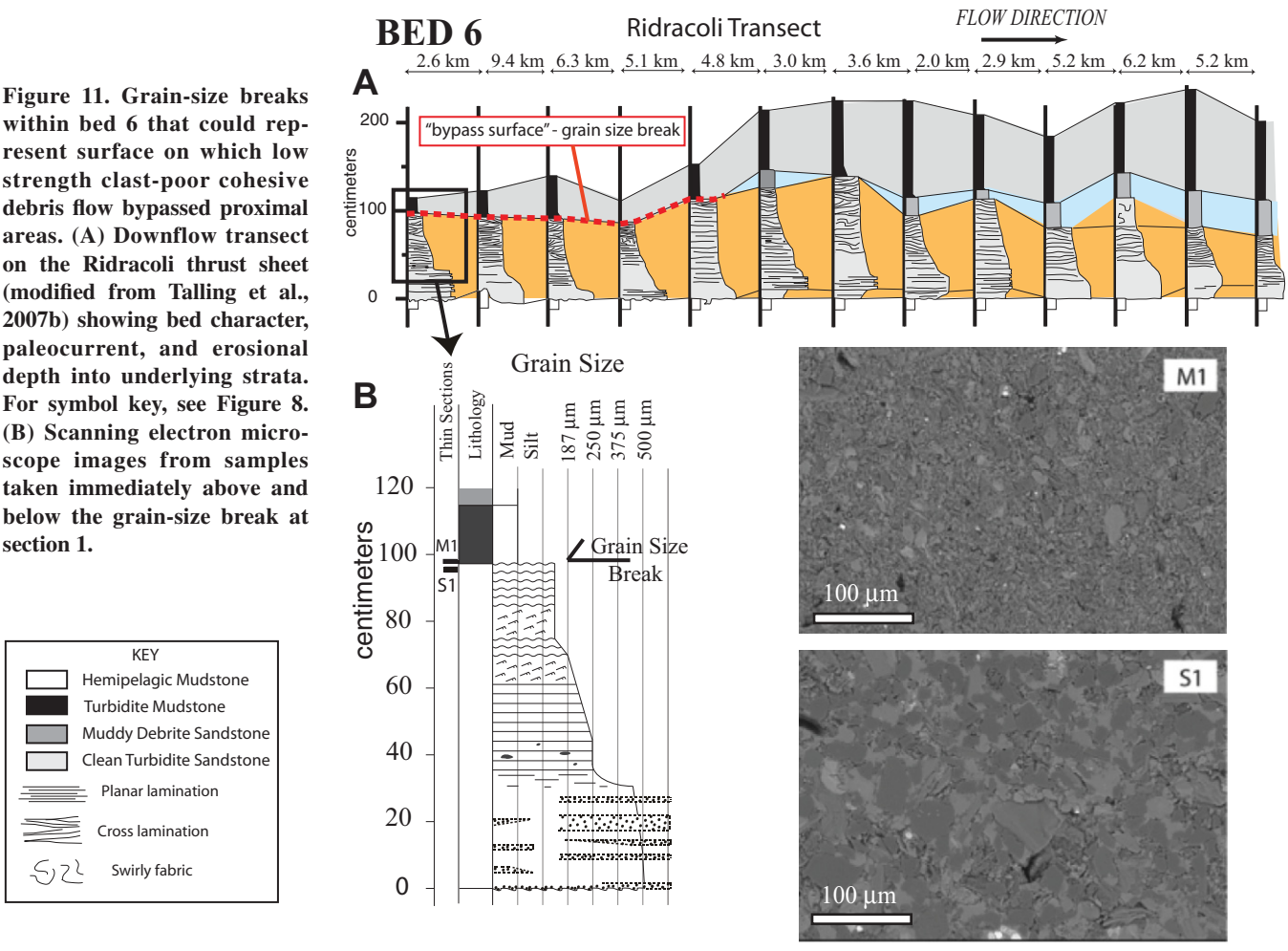

Figure 11. Grain-size breaks within bed 6 that could represent surface on which low strength clast-poor cohesive debris flow bypassed proximal areas. (A) Downflow transect on the Ridracoli thrust sheet (modified from Talling et al., 2007b) showing bed character, paleocurrent, and erosional depth into underlying strata. For symbol key, see Figure 8. (B) Scanning electron microscope images from samples taken immediately above and below the grain-size break at section 1.

Fig. 10). The range of detrital components seen in these sandstone samples is similar, again suggesting that both types of sandstone came from a broadly similar source.

DISCUSSION

Origin of Mud-Rich (Cohesive) Debris Flows

Two lines of evidence suggest that the matrix mud and mud clasts in the cohesive debris flows originated outside of the study area. The location of the base of the continental slope is not well known for the Marnoso-arenacea Formation (Ricci-Lucchi and Valmori, 1980; Gandolfi et al., 1983; Mutti et al., 1992), and this sediment could have originated either from more proximal parts of the basin plain, or from locations even further updip.

Composition of Mud Clasts

Mud-rich debrite intervals in bed 2.5 contain both turbidite mudstone and hemipelagic mudstone clasts, which can be distinguished by their color and the presence or lack of abundant foraminifera tests (Ricci Lucchi and Valmori, 1980; Amy and Talling, 2006; Talling et al., 2007a) The turbidite mudstone clasts most likely originated from outside of the study area, because bed correlations (Figs. 2–4; Amy and Talling, 2006; Talling et al., 2007a, 2007b) show that the flow responsible for bed 2.5 only eroded into underlying hemipelagic mudstone at the 109 studied locations (Figs. 4 and 10; Supplemental Fig. 2 in the Supplemental Figure File [see footnote 1]). It is possible that deeper erosion occurred at other locations in the basin plain, but this seems less likely given the large number of studied outcrops, some of which could be walked out for distances of as much as 2 km. Clast-rich debrite intervals in bed 3, and millimeter-scale clasts in clast-poor debrite intervals within beds 1 and 6, also comprise both turbidite and hemipelagic mudstone (Fig. 9). The flows responsible for beds 1, 3, and 6 are almost always underlain by hemipelagic mudstone, and only eroded into turbidite mud in a few (<3 of 109) logged sections on the Ridracoli thrust sheet (Figs. 2, 9, 11, and 12). It seems unlikely that erosion in such few locations could lead to widespread dispersion of turbidite mud clasts in beds 1, 3, and 6.

Abundant Disseminated Organic Material

Disseminated organic carbon is particularly abundant in both clast-rich and clast-poor mud-rich debrite intervals (Table 2), commonly including fragments large enough to be visible by eye. It is likely that this organic carbon material originated outside of the outcrop area, most probably as the result of slope failure of deltaic sequences. Hemipelagic mudstone intervals in the outcrop area lack visible organic carbon fragments (Talling et al., 2007a, fig. 3 therein); therefore, the high TOC fraction within the debrites (Table 2) cannot have originated through erosion of mostly or completely hemipelagic mudstone in the outcrop area. However, erosion in the basin plain may have reduced the relative fraction of organic material in matrix mud from an initially even higher value. The mud-rich matrix of the clast-rich debrite in bed 2.5 at Monte Roncole (Fig. 10; section 14) has a higher TOC content than the overlying

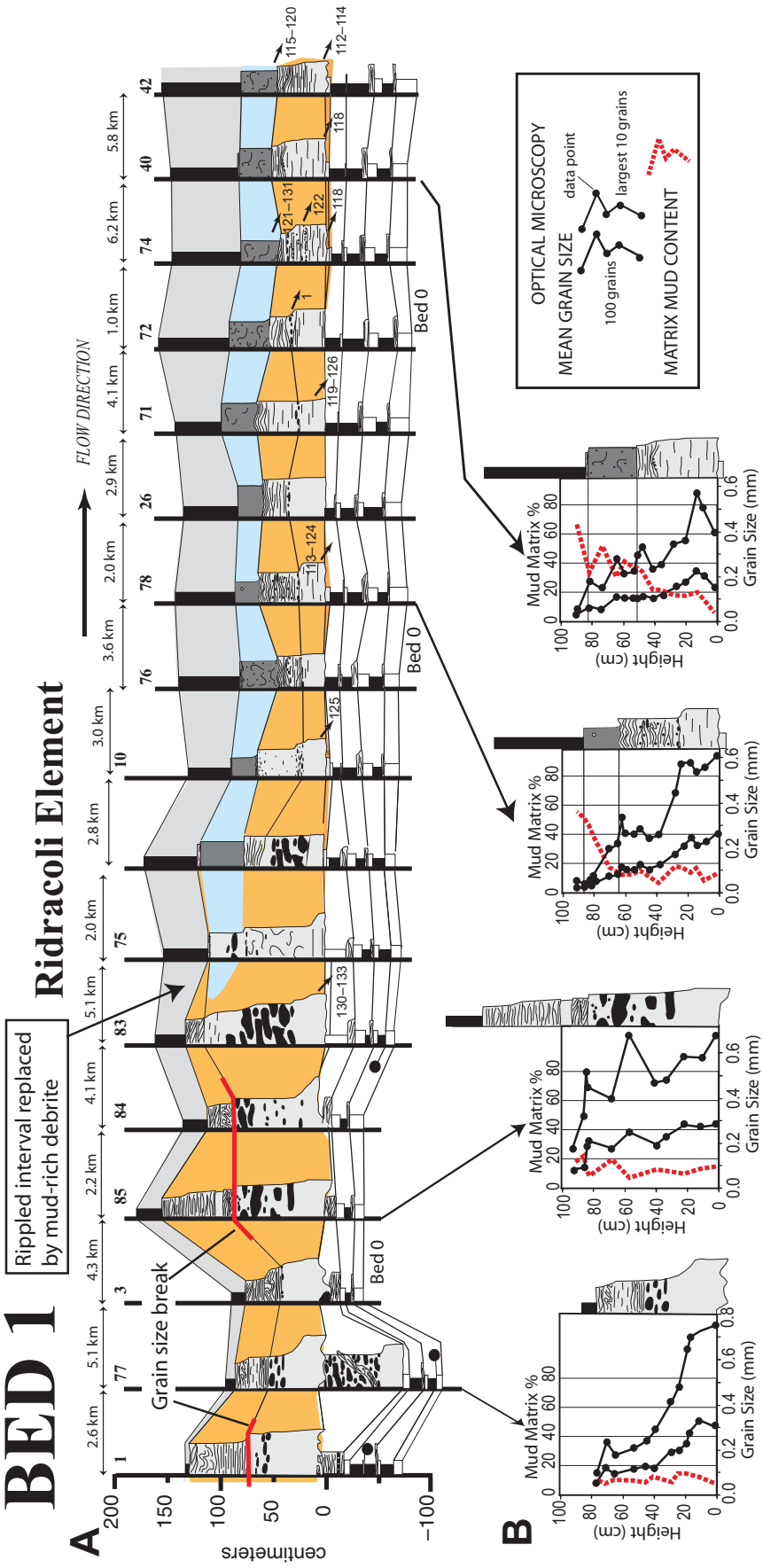

Figure 12. (A) Downflow changes in bed 1 along the Ridracoli thrust sheet, showing how thick ripple cross-laminated clean sand and mud-rich debrite sandstone are mutually exclusive. (B) Grain size and mud matrix content in bed 1 from four locations, based on optical microscopy. For symbol key, see Figure 8.

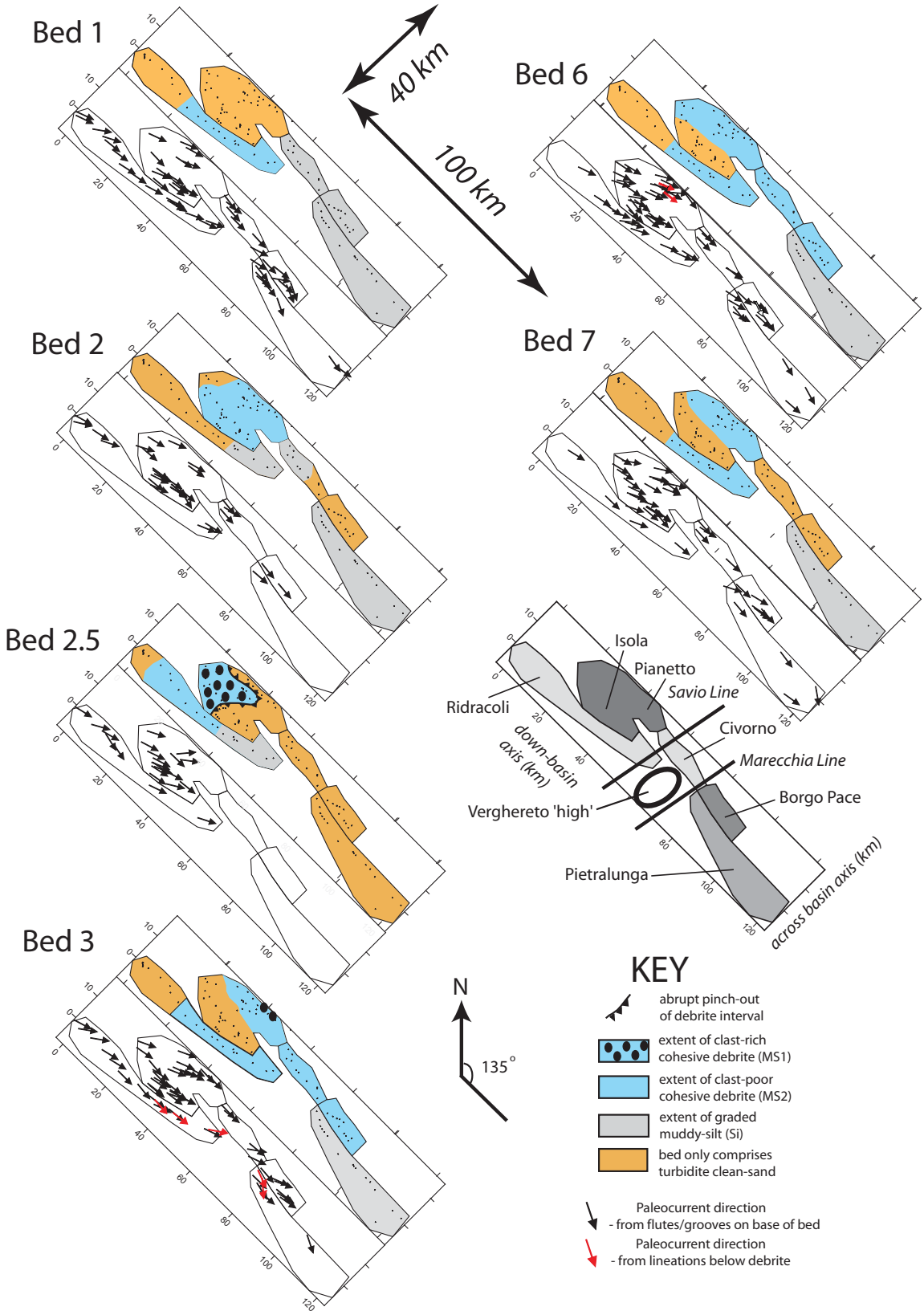

Figure 13. Planform distribution of clast-rich and clast-poor cohesive debrite intervals in individual hybrid beds within the interval above the Contessa bed. The mean paleocurrent direction at each logged section is also shown for each bed. Paleocurrent directions from the base of beds (black arrows) and paleocurrent directions from dunes or corrugations immediately below the debrite (red arrows) are distinguished. For symbol key, see Figure 8.

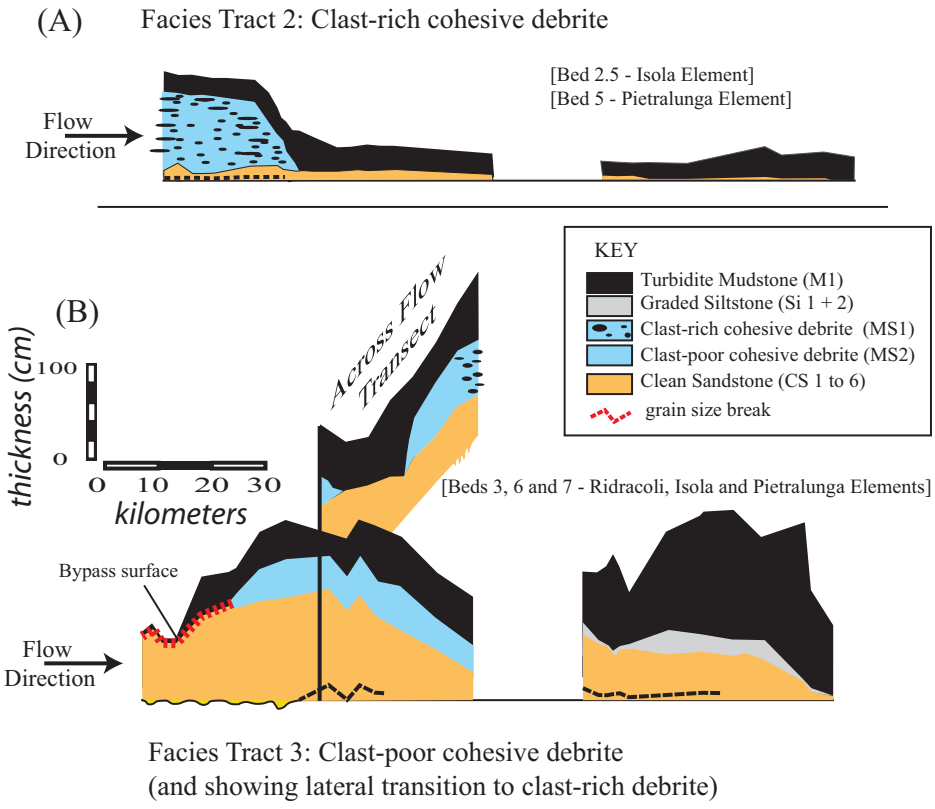

Figure 14. Summary of typical downflow cross-section geometries (facies tracts; Mutti, 1992) for hybrid beds. (A) Beds containing clast-rich cohesive debrite intervals. (B) Beds containing clast-poor cohesive debrite intervals. Facies tract 2 with clast-rich debrite is based on bed 2.5 on the Isola structural element (see Fig. 10) and bed 5 on the Pietralunga element. Facies tract 3 with clast-poor debrite is based on bed 3 (see Fig. 9), bed 6 (see Fig. 11), and bed 7 on the Ridracoli and Pietralunga structural elements. Also shown is the lateral transition from clast-poor to clast-rich cohesive debrite intervals seen in bed 3 from the Ridracoli to Isola to Pianetto structural elements (see Fig. 9).

turbidite mudstone, albeit based on only one debrite sample (Table 2). This might suggest that the debrite matrix originates directly from the original organic carbon–rich slope failure with only partial mixing of that organic carbon material into the associated turbidity current, and with relatively little addition of matrix mud lacking organics into the debrite due to erosion within the basin plain. This is consistent with the relatively large volume of cohesive debrite, and small volume of turbidite, in bed 2.5. The TOC contents in the matrix of clast-rich debrite in bed 3 and the matrix of clast-poor debrite in bed 6 at the Cigno section (Fig. 9; section 5) are broadly similar to those in the turbidite mudstone and debrite matrix, once the relative fractions of cohesive mud in the different lithologies are taken into account (Table 2). This suggests that the debris flow mud matrix and muddy turbidity current have a broadly similar source.

Mudstone clasts in the debrite commonly comprise both organic-poor hemipelagic mud and turbidite mud with abundant organics. The hemipelagic mud clasts may have originated from a source area different from that of the organic-rich matrix, or the hemipelagic mud may represent interbedded layers from the same initial sedimentary sequence.

Origin of Clast-Rich (Higher Strength) Cohesive Debrites

Where clast-rich muddy debrite intervals occur in beds 2.5, 3, 5, and 6.1, they extend to the available limit of outcrop in an upflow direction (Figs. 2, 4, 9, 10, and 13). The compositions of clasts and high organic carbon content in the matrix indicate that the debris flows originated outside the outcrop area. These higher strength debris flows therefore ran out for at least several tens of kilometers across the basin plain. Small to intermediate diameter (<~1 m) mud clasts were most likely supported mainly by matrix strength, while the largest clasts (such as the 3.2-m-long clasts in Figs. 6A, 6B) may have been supported because they are less dense than the surrounding matrix. A more detailed analysis of clast support in cohesive debris flows was provided in Talling et al. (2010). This type of intermediate strength debris flow is broadly similar to intermediate strength debris flows responsible for thicker clast-rich debrites (e.g., Piper et al., 1999; Laberg and Vorren, 2000; Tripsanas et al., 2008), but it has a lower strength that permits a longer runout across low gradients.

Origin of Clast-Poor Mud-Rich (Cohesive) Debrites

Clast-poor debrites contain millimeter-scale clasts and abundant organic carbon material that most likely originated outside the outcrop area, but the clast-poor cohesive debrite intervals are absent in the most proximal locations on the Ridracoli transect (Fig. 13). The absence of clast-poor debrites in these proximal locations may result from the cohesive debris flow path not coinciding with these locations (Fig. 17A). However, the paleocurrent data suggest that this is unlikely, especially as it must have occurred for several different beds (Fig. 13). The cohesive clast-poor debris flows may have originated outside the outcrop area, and the debris flows then bypassed the proximal outcrops without depositing debrite (Fig. 16B). A proximal grain-size break between turbidite sand and mud may be a record of such bypass, although the grain-size break also occurs in beds lacking debrites (e.g., bed 4; Amy and Talling, 2006). However, we might expect the debris flow to have left at least a thin deposit in the proximal basin, debrite deposit thickness being determined by seafloor gradient and debris flow strength.

In Amy and Talling (2006), a process by which the cohesive debris flows formed from initial turbidity currents through erosion of the seafloor within the outcrop (Fig. 17C) was favored; this erosion would produce areas of deep grooves as deep as 10 cm (Fig. 5B). The flow transformation resulted from addition of cohesive mud into the basal part of the flow as the mud clasts disaggregated. This increase in cohesive mud content damped turbulence and caused a transition into laminar flow. However, the mud-clast composition suggests that at least some clasts originated outside the outcrop area. In addition, we might expect the flow to be faster and more erosive on steep slopes in the early path of the flow path, such that the flow was more erosive further upslope. It is also unclear why the cohesive debrite interval could be separated from the surface of basal erosion by an interval of clean turbidite sand (Figs. 9, 11, and 12). It is therefore likely that

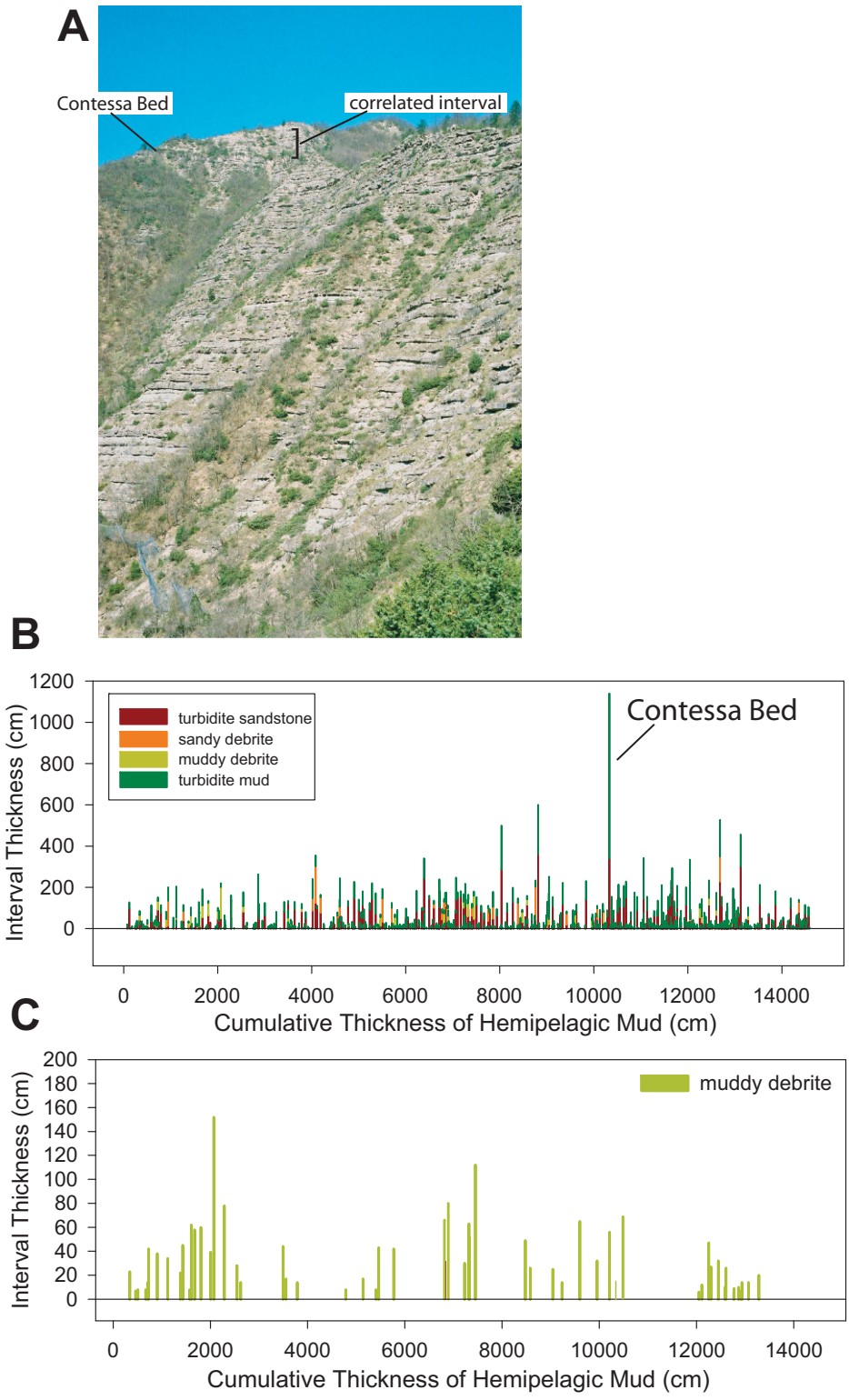

Figure 15. (A) Outcrop photograph showing lower ~300 m of 419-m-long Cabelli section in which every bed is exposed. The Contessa megaturbidite marker bed is indicated, together with the overlying interval of strata in which beds were correlated between 108 other sections. (B) Plot showing the thickness of beds, and the thickness of different facies within beds, against the cumulative thickness of hemipelagic mud from the base of the section. The cumulative thickness of hemipelagic mud is a proxy for time. (C) Plot showing the frequency and thickness of mud-rich debrite sandstone intervals.

neither clast-rich nor clast-poor debris flows originated in this fashion.

A final explanation for the lack of debrites in proximal areas is that a flow transformation occurred within the basin from fully turbulent turbidity current to (laminar) debris flow, but that the flow transformation was not a result of erosion of muddy substrate within the outcrop area (Figs. 17D, 17E). The flow transformation occurred as the flow slowed, such that cohesive bonds developed between the existing cohesive fine-mud particles within the flow (Baas et al., 2009, 2011; Sumner et al., 2008, 2009). These cohesive bonds increased the viscosity of the muddy fluid, and led to further flow deceleration, such that turbulence collapsed to leave a final phase of laminar flow. Recent laboratory experiments suggest that such a collapse of turbulence, and resulting transition into laminar plug flow, may be common in flows with small but sufficient mud content as their velocity decreases (Baas et al., 2009, 2011; Sumner et al., 2009, 2012; Talling et al., 2012a). The initial turbidity current may have bypassed sediment, as recorded by the grain-size break between turbidite sand and mud (Fig. 11). Alternatively, and perhaps more likely, the initial turbidity current may have deposited the intervals of ripple cross-laminated sand that terminate once debrite deposition begin (Fig. 12). Abrupt downflow transitions from thick ripple cross-laminated clean sandstone to mud-rich debrite sandstone favor such a model. The initial turbidity current would need to be sufficiently vigorous to support millimeter-scale mud clasts, bearing in mind that mud clasts tend to have a significantly lower unit density than quartz sand.

Debris flows formed by such flow transformation may have behaved in two different ways (Figs. 17D, 17E). (1) The debris flow may have run out for tens of kilometers across the basin plain to produce an extensive cohesive debrite (Fig. 17D). The low strength clast-poor debris flow would have had to move slowly to avoid mixing with surrounding seawater (Talling et al., 2002). (2) The low strength debris flow may have formed locally, close to the site of eventual debrite deposition (Fig. 17E). In this model, the location of the flow transformation would migrate across the basin plain, and the cohesive debris flows would not run out for long distances. Experiments involving low strength mixtures of cohesive fine mud qualitatively show how easily such low strength (<5 Pa) mixtures mix with surrounding water when stirred gently. However, without more quantitative constraints on rheology and speed of the ancient debris flows it is difficult to determine whether the low strength debris flows formed locally, or ran out slowly for long distances.

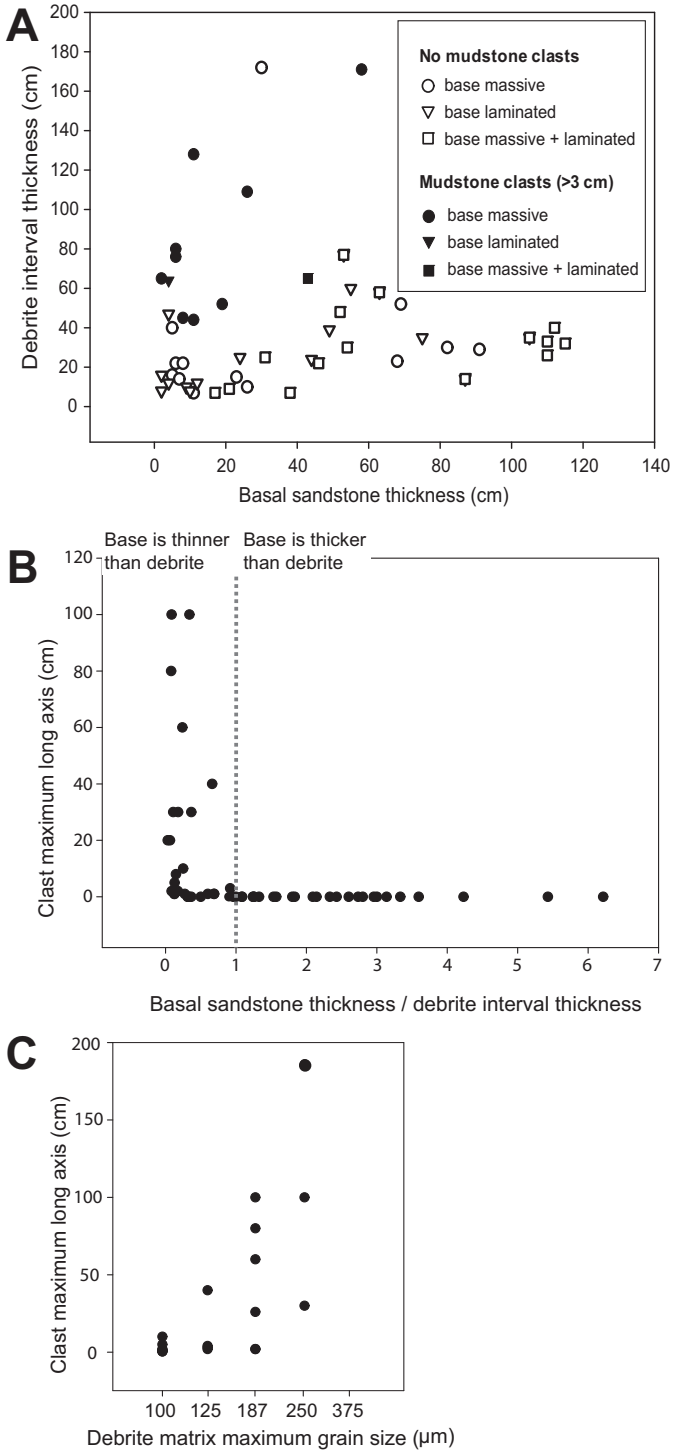

Figure 16. Plots summarizing the character of beds comprising both mud-rich debrite sandstone intervals and encasing turbidite sandstone and mudstone in the longer Cabelli section (see Fig. 15). Each symbol represents a separate bed. (A) Plot showing muddy debrite interval thickness and basal clean sandstone thickness for muddy debrites that are clast rich or clast poor. The figure shows whether the basal clean sandstone in the bed is structureless, laminated, or structureless overlain by laminated. (B) Plot showing the relationship between clast sixe within the muddy debrite, and the relative thickness of the muddy debrite in comparison to the basal clean sand. Muddy debrites with larger clasts tend to have a relatively thin basal clean sandstone. (C) Plot showing the size of the largest clasts and the size of larger sand grains (measured with a grain-size comparator card) in the muddy debrite intervals.

Lateral Changes from Clast-Rich to Clast-Poor Cohesive Debris Flow

Lateral changes are observed from clast-rich debris flow that most likely originated outside the outcrop area, to clast-poor debris flows that most likely originated via transformation from turbidity currents within the study area (Figs. 9 and 14). These lateral changes in how the debris flows formed and ran out was probably a result of lateral changes in mud content and cohesive strength.

Depositional Processes of Basal Clean Sandstone and Cohesive Debris Flow Mobility

The mud-rich debrites are overlain by turbidite mud or thin intervals of ripple cross-laminated fine sand. These overlying intervals were deposited by dilute turbidity currents and muddy turbidity currents that composed the rear part of the overall flow event.

The cohesive mud-rich debrites are underlain by different types of clean sand, and it is important to understand how this sand was deposited in order to understand the complete flow event, in particular, whether the basal clean sand was deposited by turbidity current or by another process. It is also important to determine whether the basal clean sand could have lubricated the cohesive debris flows, thereby increasing debris flow runout, as suggested by Haughton et al. (2009).

Basal Clean Sandstone Below Clast-Rich (Higher Strength) Cohesive Debrites

The basal clean sand interval is typically relatively thin (<10 cm), and comprises two distinct parts separated by a grain-size break (Figs. 10 and 14). The first part comprises structureless clean sand and forms all of the basal clean sand in most proximal locations, and it is typically normally graded (Fig. 10). The second part comprises much finer grained and ripple cross-laminated clean sand that appears at the very base of the bed just before the pinch-out of the cohesive debrite interval. This interval can be inversely graded (Fig. 10).

The structureless clean sand abruptly fines, becomes planar-laminated, and then pinches out near the termination of the overlying muddy clast-rich debrite sand in bed 2.5 (Fig. 10). This suggests that structureless basal clean sand is closely linked to deposition of the overlying mud-rich debrite. Two hypotheses explain how the structureless clean sand could be deposited. (1) The clean sand was deposited by a high-density turbidity current that ran ahead of the cohesive debris flow, but was fed by sand mixed from the debris flow. Therefore, the forerunning turbidity current stopped soon after the

TABLE 2. TOTAL ORGANIC CARBON CONTENT NORMALIZED BY MUD VOLUME FRACTION

Section	Bed number	Lithology	TOC (%)	Mud (volume fraction)	TOC (%)/Mud
Monte Roncole	2.5	basal clean sand	0.077	0.10	0.77
Monte Roncole	2.5	Clast-rich muddy debrite sand	0.523	0.40	1.30
Monte Roncole	2.5	turbidite mud	0.275	0.80	0.34
Monte Roncole	2.5	turbidite mud	0.344	0.80	0.43
Cigno	6	basal clean sand	0.030	0.10	0.30
Cigno	6	basal clean sand	0.036	0.10	0.36
Cigno	6	basal clean sand	0.081	0.10	0.81
Cigno	6	Clast-poor muddy debrite sand	0.524	0.40	1.31
Cigno	6	Clast-poor muddy debrite sand	0.257	0.40	0.64
Cigno	6	Clast-poor muddy debrite sand	0.384	0.40	0.96
Cigno	6	turbidite mud	0.657	0.80	0.82
Cigno	6	turbidite mud	0.650	0.80	0.81
Cigno	6	turbidite mud	0.706	0.80	0.88
Cigno	3	basal clean sand	0.024	0.10	0.24
Cigno	3	basal clean sand	0.032	0.10	0.31
Cigno	3	basal clean sand	0.042	0.10	0.41
Cigno	3	Clast-rich muddy debrite sand	0.287	0.40	0.72
Cigno	3	Clast-rich muddy debrite sand	0.290	0.40	0.72
Cigno	3	turbidite mud	0.574	0.80	0.72
Cigno	3	turbidite mud	0.649	0.80	0.81
Cigno	3	turbidite mud	0.649	0.80	0.81

Note: Data from text Figure 7. TOC—total organic carbon.

cohesive debris flow stopped and was closely linked to the debris flow. (2) However, two different sets of laboratory experiments suggest that the normally graded structureless clean sand formed in a different way, from sand that settled out from the matrix of the debris flow. Sumner et al. (2009) found that settling of sand from the debris flow plug could occur during the later stages of debris flow motion, or for some time after the debris flow had stopped moving. The thickness of the basal clean sand, as a fraction of the overlying debris flow, was broadly similar to that seen in bed 2.5, as were the relative sizes of sand grains in the basal sand and remaining in the mud-rich debrite. Late-stage settling of larger sand-sized grains was also reported in Marr et al. (2001). In the Sumner et al. (2009) experiments, the late-stage settling of sand occurred from debris flows with very low strength (<~10 Pa), and was not observed in higher strength debris flows. It is therefore puzzling that basal clean sand layers formed in this way are seen only for the intermediate strength clast-rich debris flows, and not the clast-poor debris flows inferred to have low strength. However, it is a likely explanation for the structureless basal clean sands that pinch out in the same place as overlying cohesive clast-rich debrite (Talling et al., 2010), as such late-stage settling appears to be a rather general property of lower strength cohesive debris flow experiments.

The thin ripple cross-laminated sand in bed 2.5 extends far beyond the mud-rich debrite, and these sedimentary structures clearly indicate deposition by a dilute turbidity current that ran out far beyond the cohesive debris flow (Fig. 10; Supplemental Fig. 2 in the Supplemental Figure File [see footnote 1]). The appearance of the ripple cross-laminated sand at the base of the bed can be explained by rapid deceleration during the final stages of the debris flow. The low-density turbidity current was initially slower than the cohesive debris flow and formed the rear of the event (and hence was deposited above the debrite within the bed). However, as the debris flow slowed abruptly, the low-density turbidity current then ran ahead to form the front of the flow (and deposit at the base of the bed).

Basal Clean Sandstone Below Clast-Poor (Low Strength) Cohesive Debrite

Basal clean-sand intervals beneath clast-poor mud-rich debrites comprise parallel or wavy (crenulated) planar laminae or dune-scale (20–90 cm wavelength) cross-laminae (Amy and Talling, 2006; Talling et al., 2007b; Sumner, 2009). These basal clean sand intervals are normally graded and record incremental deposition by turbidity currents that ran ahead of the trailing debris flow. The parallel planar laminae and dune-scale cross-laminae record no evidence of dewatering and soft-sediment deformation. The wavy (crenulated) laminae most likely result from dewatering that deformed the laminae, but such dewatering was limited, as the laminations are subparallel and not convolute and overturned.

Crenulated laminations may record limited dewatering in some locations below the debris flow, but in many locations there is no evidence of dewatering of the basal clean sand. The cohesive debris flows were therefore capable of running out for long distances without being lubricated by dewatering of the basal sand, as implied by theoretical analyses of low strength debris flow motion (Talling et al., 2010).

The basal turbidite clean sandstone commonly has a shape with a broad thickness maximum (Figs. 9, 11, and 14; Talling et al., 2007b). This same shape is observed in turbidite sandstone intervals below debrite sandstone intervals (beds 3 and 6), and in beds that lack any debrite sandstone (bed 4). This consistent shape suggests that these turbidity currents evolved in a way that was largely independent of the trailing low strength cohesive debris flow.

Transition From Basal Clean Sand to Muddy Debrite Sand

The transition from basal clean sand to overlying mud-rich debrite is either very sharp, or occurs over a thickness of <~2 cm. Haughton et al. (2009) proposed that an interval with repeated banding of mud-poor and mud-rich sand (their H3 interval) commonly occurs between basal clean sand intervals and overlying mud-rich debrite sand intervals in hybrid turbidite-debrite beds. However, such repeated banded intervals are not seen in the Marnoso-arenacea Formation.

CONCLUSIONS

Previous work showed that hybrid beds comprising turbidite and mud-rich cohesive debrite were common within an ~30-m-thick stratigraphic interval, and that low strength (clast poor) and intermediate strength (clast rich) debrite occurred in downflow-trending facies tracts with substantially different geometries. Low strength debrite has no clasts or small (<5 mm) mud chips, and is underlain by thick graded turbidite sand. It grades downflow into fine silt within the distal basin plain. Intermediate strength debrite has large and abundant clasts, and is <~2 m thick. Clast-rich debrite is underlain by a thin structureless clean sand, and both cohesive debrite and basal structureless clean sand pinch out abruptly at the same location. A single hybrid bed can locally contain both clast-rich and clast-poor debrite, and be in different positions across flow, most likely due to lateral changes in debris flow strength. Past work also showed that both types of debrite are absent in the most proximal outcrops for the 30-m-thick interval of correlated beds.

We have shown that hybrid beds are common in a much thicker (419 m) stratigraphic interval than studied previously, and the same two types of debrite occur. Hybrid flows transported large volumes (to 10 km^3 per flow) of sediment into this basin plain over a prolonged period of time. New information on the planform shape of mud-rich debrites shows that clast-rich and clast-poor

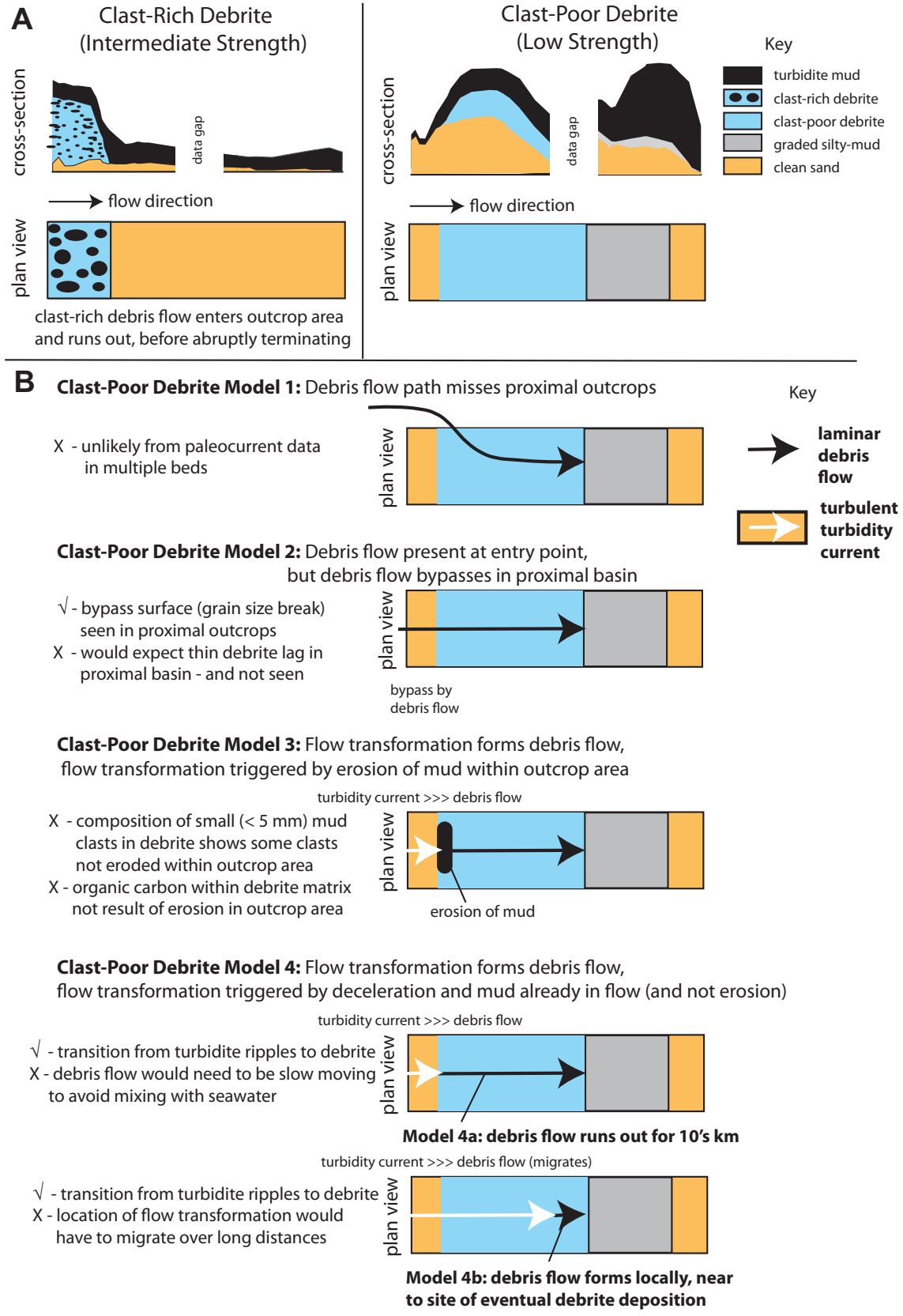

Figure 17. (A) Simplified summary of the cross-sectional and plan-form shape of hybrid beds containing clast-rich and clast-poor cohesive debrites. (B) Potential models for the origin of clast-poor debrites, which are absent in the proximal part of the hybrid bed, noting aspects of the field evidence in favor (√) or against (X) each of the models.

debrites have substantially different shapes; however, each of the two types of debrite has a consistent shape. Clast-poor debrites form two tongues at the margins of the outcrop, perhaps due to a subtle basin-floor topography. Clast-rich debrite occurs as a single tongue located nearer the basin center. Both types of debrite are absent in the most proximal and distal outcrops, and are most common in the mid-basin. Intermediate strength debrites are underlain by a thin layer of structureless clean sandstone that may have settled out from the debris flow at a late stage, as seen in laboratory experiments, or have been deposited by a fore-running turbidity current closely linked to the debris flow. Low strength debrites can infill relief created by underlying dune crests, suggesting gentle emplacement. Dewatering of underlying basal clean sand did not cause long runout of debris flows in this location.

The cohesive debris flows did not originate within the basin due to erosion of underlying muddy seafloor, as previously thought to be most likely (see Amy and Talling, 2006). Mapping of underlying thin bedded intervals shows that some mud clasts in the debrites originated outside the outcrop area, as did abundant carbonaceous matter within the debrite matrix. Intermediate strength (clast rich) debris flows entered the study area as debris flows that ran out for tens of kilometers across the basin floor. Low strength (clast-poor) debris flows most likely originated through transformation from an initially turbulent mud-rich suspension, which deposited no sediment in proximal areas. It is unclear whether low strength cohesive debris flows ran out for long distances, or formed close to the site of eventual debrite deposition. The field data show the complex nature of hybrid flows even in a basin plain with little topography. Sediment within the hybrid flows was far traveled from outside the study area, and the dynamics and deposit geometry varied with debris flow cohesive strength.

ACKNOWLEDGMENTS

This work was part of a UK-TAPS (Turbidite Architecture and Process Studies) project, funded by NERC (Natural Environment Research Council) Ocean Margins LINK grants NER/T/S/2000/0106 and NER/M/S/2000/00264, and cosponsored by ConocoPhillips, BHP Billiton, and Shell. We thank Gianni Zuffa and Franco Ricci-Lucchi (Bologna University) and Luca Martelli (Emilia Romagna Geological Survey) for advice on field work in northern Italy. Bed correlations presented in this study were made possible by the outstanding mapping of marker beds by the Geological Survey of Italy and pioneering studies of the Marnoso-arenacea Formation led by Ricci-Lucchi and Martelli. We also thank Mike Rogerson (University of Hull) and Tanja Kouwenhoven (Utrecht University) for their efforts to disaggregate samples and analyze benthic foraminifera assemblages. Comments by Gillian Apps (BP), Dominic Armitage, David McGee, and Bill Morris (ConocoPhillips), Ian Westlake and Chris Lerch (BHP Billiton), Zoltan Sylvester and Carlos Pirmez (Shell), Jaco Baas (Bangor University), Peter Haughton (University College Dublin), Jeffrey Peakall (University of Leeds), Richard Hiscott (Memorial University), David Piper (Bedford Oceanography Institute), and two anonymous reviewers were greatly appreciated. Bill Normark, to whom this volume is dedicated, provided inspiration through his varied and substantial body of work.

REFERENCES CITED

Amy, L.A., and Talling, P.J., 2006, Anatomy of turbidites and linked debrites based on long distance (120 × 30 km) bed correlation, Marnoso Arenacea Formation, northern Apennines, Italy: Sedimentology, v. 53, p. 161–212, doi:10.1111/j.1365-3091.2005.00756.x.

Amy, L.A., Talling, P.J., Peakall, J., Wynn, R.B., and Arzola Thynne, R.G., 2005, Bed geometry used to test recognition criteria of turbidites and (sandy) debrites: Sedimentary Geology, v. 179, p. 163–174, doi:10.1016/j.sedgeo.2005.04.007.

Amy, L.A., Peachey, S.A., Gardiner, A.A., and Talling, P.J., 2009, Prediction of hydrocarbon recovery from turbidite sandstones with linked debrite facies: Numerical flow-simulation studies: Marine and Petroleum Geology, v. 26, p. 2032–2043, doi:10.1016/j.marpetgeo.2009.02.017.

Baas, J.H., Best, J.L., Peakall, J., and Wang, M., 2009, A phase diagram for turbulent transitional and laminar clay suspension flows: Journal of Sedimentary Research, v. 79, p. 162–183, doi:10.2110/jsr.2009.025.

Baas, J.H., Best, J.L., and Peakall, J., 2011, Depositional processes, bedform development and hybrid bed formation in rapidly decelerated cohesive (mud-sand) sediment flows: Sedimentology, v. 58, p. 1953–1987, doi:10.1111/j.1365-3091.2011.01247.x.

Frenz, M., Wynn, R.B., Georgiopoulou, A., Bender, V.B., Hough, G., Masson, D.G., Talling, P.J., and Cronin, B.T., 2008, Unravelling turbidite basin fill complexity: A case study from the late Quaternary turbidite fill of the Agadir Basin, offshore Atlantic Morocco: International Journal of Earth Sciences, v. 98, p. 721–733, doi:10.1007/s00531-008-0313-4.

Gandolfi, G., Paganelli, L., and Zuffa, G.G., 1983, Petrology and dispersal directions in the Marnoso Arenacea Formation (Miocene, northern Apennines): Journal of Sedimentary Petrology, v. 53, p. 493–507.

Haughton, P.D.W., Barker, S.P., and McCaffrey, W., 2003, 'Linked' debrites in sand-rich turbidite systems—Origin and significance: Sedimentology, v. 50, p. 459–482, doi:10.1046/j.1365-3091.2003.00560.x.

Haughton, P.D.W., Davis, C., McCaffrey, W., and Barker, S.P., 2009, Hybrid sediment gravity flow deposits—Classification, origin and significance: Marine and Petroleum Geology, v. 26, p. 1900–1918, doi:10.1016/j.marpetgeo.2009.02.012.

Hiscott, R.N., and Middleton, G.V., 1979, Depositional mechanics of the thick-bedded sandstones at the base of a submarine slope, Tourelle Formation (Lower Ordovician), Quebec, Canada, *in* Doyle, L.J., and Pilkey, O.H., eds., Geology of continental slopes: Society of Economic Paleontologists and Mineralogists Special Publication 27, p. 307–326, doi:10.2110/pec.79.27.0307.

Hiscott, R.N., and Middleton, G.V., 1980, Fabric of coarse deep-water sandstones, Tourelle Formation, Quebec, Canada: Journal of Sedimentary Research, v. 50, p. 703–722, doi:10.1306/212F7AC7-2B24-11D7-8648000102C1865D.

Hodgson, D.M., 2009, Distribution and origin of hybrid beds in sand-rich submarine fans of the Tanqua depocentre, Karoo Basin, South Africa: Marine and Petroleum Geology, v. 26, p. 1940–1957, doi:10.1016/j.marpetgeo.2009.02.011.

Ito, M., 2008, Downfan transformation from turbidity currents to debris flows at a channel-to-lobe transitional zone: The lower Pleistocene Otadai Formation, Boso Peninsula, Japan: Journal of Sedimentary Research, v. 78, p. 668–682, doi:10.2110/jsr.2008.076.

Jackson, C.A.-L., Adli Zakaria, A., Johnson, H., Tongkul, F., and Crevello, P.D., 2009, Sedimentology, stratigraphic occurrence and origin of linked debrites in the West Crocker Formation (Oligo-Miocene), Sabah, NW Borneo: Marine and Petroleum Geology, v. 26, p. 1957–1973, doi:10.1016/j.marpetgeo.2009.02.019.

Laberg, J.S., and Vorren, T.O., 2000, Flow behaviour of the submarine glacigenic debris flows on the Bear Island Trough Mouth Fan, western Barents Sea: Sedimentology, v. 47, p. 1105–1117, doi:10.1046/j.1365-3091.2000.00343.x.

Lowe, D.R., 1982, Sediment gravity flows; 2, Depositional models with special reference to high density turbidity currents: Journal of Sedimentary Research, v. 52, p. 279–298, doi:10.1306/212F7F31-2B24-11D7-8648000102C1865D.

Marr, J.G., Harff, P.A., Shanmugam, G., and Parker, G., 2001, Experiments on subaqueous sandy gravity flows: The role of clay and water content in flow dynamics and depositional structures: Geological Society of America Bulletin, v. 113, p. 1377–1386, doi:10.1130/0016-7606(2001)113<1377:EOSSGF>2.0.CO;2.

Milliman, J.D., and Syvitski, J.P.M., 1992, Geomorphic tectonic controls of sediment discharge to the ocean—The importance of small mountain rivers: Journal of Geology, v. 100, p. 525–544, doi:10.1086/629606.

Mutti, E., 1992, Turbidite Sandstones: Istituto di Geologia Università di Parma & AGIP, 275 p.

Mutti, E., Ricci Lucchi, F., and Roveri, M., 2002, Revisiting turbidites of the Marnoso Arenacea Formation and their basin-margin equivalents: Problems with classic models: 64th EAGE Conference and Exhibition Excursion Guidebook: Parma, Italia, Editrice Campus, 52 p.

Muzzi Magalhaes, P., and Tinterri, R., 2010, Stratigraphy and depositional setting of slurry and contained (reflected) beds in the Marnoso-arenacea Formation (Langhian-Serravallian) northern Apennines, Italy: Sedimentology, v. 57, p. 1685–1720, doi:10.1111/j.1365-3091.2010.01160.x.

Nielsen, T., Shew, R.D., Steffens, G.S., and Studlick, J.R.J., 2007, Atlas of deepwater outcrops: American Association of Petroleum Geologists Studies in Geology 56, 504 p.

Piper, D.J.W., Cochonat, P., and Morrison, M.L., 1999, The sequence of events around the epicentre of the 1929 Grand Banks earthquake: Initiation of the debris flows and turbidity current inferred from side scan sonar: Sedimentology, v. 46, p. 79–97, doi:10.1046/j.1365-3091.1999.00204.x.

Pyles, D.R., and Jennette, D.C., 2009, Geometry and architectural associations of co-genetic debrite-turbidite beds in basin margin strata, Carboniferous Ross Sandstone (Ireland): Applications to reservoirs located on the margins of structurally confined submarine fans: Marine and Petroleum Geology, v. 26, p. 1940–1957, doi:10.1016/j.marpetgeo.2009.02.018.

Reeder, M.S., Rothwell, D.G., and Stow, D.A.V., 2000, Influence of sea level and basin physiography on emplacement of the late Pleistocene Herodotus Basin megaturbidite, SE Mediterranean Sea: Marine and Petroleum Geology, v. 17, p. 199–218, doi:10.1016/S0264-8172(99)00048-3.

Ricci-Lucchi, F., and Valmori, E., 1980, Basin-wide turbidites in a Miocene, over-supplied deep-sea plain: A geometrical analysis: Sedimentology, v. 27, p. 241–270, doi:10.1111/j.1365-3091.1980.tb01177.x.

Shanmugam, G., and Moiola, R.J., 1995, Reinterpretation of depositional processes in a classic flysch sequence (Pennsylvanian Jackfork Group), Ouachita Mountains, Arkansas and Oklahoma: American Association of Petroleum Geologists Bulletin, v. 79, p. 672–695.

Sumner, E.J., 2009, Settling dynamics and deposits of sheared sand-mud suspensions: Implications for the interpretation of submarine gravity flow deposits [Ph.D. thesis]: Bristol, UK, University of Bristol, 164 p.

Sumner, E., Amy, L., and Talling, P.J., 2008, Deposit structure and processes of sand deposition from a decelerating sediment suspension: Journal of Sedimentary Research, v. 78, p. 529–547, doi:10.2110/jsr.2008.062.

Sumner, E.J., Talling, P.J., and Amy, L.A., 2009, The deposits of flows transitional between turbidity currents and

debris flow: Geology, v. 37, p. 991–994, doi:10.1130/G30059A.1.

Sumner, E.J., Talling, P.J., Amy, L.A., Wynn, R.B., Stevenson, C., and Frenz, M., 2012, Facies architecture of ancient and modern basin-plain turbidites: Similarities and differences to existing models and implications for sediment gravity flow processes: Sedimentology, doi:10.1111/j.1365-3091.2012.01329.x.

Sylvester, Z., and Lowe, D.R., 2004, Textural trends in turbidites and slurry beds from the Oligocene flysch of the Carpathians, Romania: Sedimentology, v. 51, p. 945–972, doi:10.1111/j.1365-3091.2004.00653.x.

Talling, P.J., Peakall, J., Sparks, R.S.J., O'Cofaigh, C., Dowdeswell, J.A., Felix, M., Wynn, R.B., Baas, J., Hogg, A.J., Masson, D.G., Taylor, J., and Weaver, P.P.E., 2002, Experimental constraints on shear mixing rates and processes: Implications for the dilution of submarine debris flows, *in* Dowdeswell, J.A., and O'Cofaigh, C., eds., Glacier influenced sedimentation on high latitude continental margins: Geological Society [London] Special Publication 203, p. 89–103, doi:10.1144/GSL.SP.2002.203.01.06.

Talling, P.J., Amy, L.A., Wynn, R.B., Peakall, J., and Robinson, M., 2004, Beds comprising debrite sandwiched within co-genetic turbidite: Origin and widespread occurrence in distal depositional environments: Sedimentology, v. 51, p. 163–194, doi:10.1111/j.1365-3091.2004.00617.x.

Talling, P.J., Amy, L.A., Wynn, R.B., Blackbourn, G., and Gibson, O., 2007a, Turbidity current evolution deduced from extensive thin turbidites: Marnoso Arenacea Formation (Miocene), Italian Apennines: Journal of Sedimentary Research, v. 77, p. 172–196, doi:10.2110/jsr.2007.018.

Talling, P.J., Amy, L.A., and Wynn, R.B., 2007b, New insight into the evolution of large volume turbidity currents; Comparison of turbidite shape and previous modelling results: Sedimentology, v. 54, p. 737–769, doi:10.1111/j.1365-3091.2007.00858.x.

Talling, P.J., and 12 others, 2007c, Onset of submarine debris flow deposition far from original giant landslide: Nature, v. 450, p. 541–544, doi:10.1038/nature06313.

Talling, P.J., Wynn, R.B., Rixon, R., Sumner, E.J., and Schmidt, D., 2010, How did submarine flows transport boulder sized mud intra-clasts to the fringes of the Mississippi Fan?: Journal of Sedimentary Research, v. 80, p. 829–851, doi:10.2110/jsr.2010.076.

Talling, P.J., Sumner, E.J., Masson, D.G., and Malgesini, G., 2012a, Subaqueous sediment density flows: Depositional processes and deposit types: Sedimentology, doi:10.1111/j.1365-3091.2012.01353.x.

Talling, P.J., Malgesini, G., and Felletti, F., 2012b, Can liquefied submarine debris flows deposit clean sandstone over large areas? Field evidence from the Marnoso-Arenacea Formation, Italian Apennines: Sedimentology, doi:10.1111/j.1365-3091.2012.01353.x.

Tripsanas, E.K., Piper, D.J.W., Jenner, K.A., and Bryant, W.R., 2008, Submarine mass-transport facies: New perspectives on flow processes from cores on the eastern North American margin: Sedimentology, v. 55, p. 97–136, doi:10.1111/j.1365-3091.2007.00894.x.

Wood, A., and Smith, A.J., 1958, The sedimentation and sedimentary history of the Aberystwyth Grits (Upper Llandoverian): Geological Society of London Quarterly Journal, v. 114, p. 163–195, doi:10.1144/gsjgs.114.1.0163.

Wynn, R.B., Weaver, P.P.E., Masson, D.G., and Stow, D.A.V., 2002, Turbidite depositional architecture across three inter-connected deep-water basins on the Northwest African Margin: Sedimentology, v. 49, p. 669–695, doi:10.1046/j.1365-3091.2002.00471.x.

Zeng, J., Lowe, D.R., Prior, D.B., Wiseman, W.J.J., and Bornhold, B.D., 1991, Flow properties of turbidity currents in Bute Inlet, British Colombia: Sedimentology, v. 38, p. 975–996, doi:10.1111/j.1365-3091.1991.tb00367.x.

Geosphere

Planform geometry, stacking pattern, and extrabasinal origin of low strength and intermediate strength cohesive debris flow deposits in the Marnoso-arenacea Formation, Italy

P.J. Talling, G. Malgesini, E.J. Sumner, L.A. Amy, F. Felletti, G. Blackbourn, C. Nutt, C. Wilcox, I.C. Harding and S. Akbari

Geosphere 2012;8;1207-1230
doi: 10.1130/GES00734.1

Notes